Classification:
BIOLOGICAL SCIENCES

Title:
CRISPR/Cas9 knockouts reveal genetic interaction between strain-transcendent erythrocyte determinants of *Plasmodium falciparum* invasion

Author affiliation:
Usheer Kanjee[a]
Christof Grüring[a]
Mudit Chaand[a]
Kai-Min Lin[b]
Elizabeth Egan[a,c]
Jale Manzo[a]
Patrick L. Jones[d]
Tiffany Yu[a]
Robert Barker Jr[d]
Michael P. Weekes[b]
Manoj T. Duraisingh[a]

(a) Department of Immunology and Infectious Diseases, Harvard T.H. Chan School of Public Health, Boston, MA, 02115, USA
(b) Cambridge Institute for Medical Research, Cambridge, CB2 OXY, United Kingdom
(c) Current address: Department of Pediatrics, Stanford University School of Medicine, Stanford, CA, USA
(d) Sanofi-Genzyme, Waltham, MA

Corresponding author:
Manoj T. Duraisingh
Department of Immunology and Infectious Diseases
Harvard T.H. Chan School of Public Health
FXB Room 205
Boston, MA, 02115, USA
mduraisi@hsph.harvard.edu
Phone: (617) 432-2675

Keywords:
BSG, CD44, CRISPR/Cas9, *Plasmodium falciparum*, parasite invasion

Abstract (250 words):

During malaria blood stage infections, *Plasmodium* parasites interact with the red blood cell (RBC) surface to enable invasion followed by intracellular proliferation. Critical factors involved in invasion have been identified using biochemical and genetic approaches including specific knockdowns of genes of interest from primary CD34+ hematopoietic stem cells (cRBCs). Here, we report the development of a robust *in vitro* culture system to produce RBCs that allow for generation of gene knockouts via CRISPR/Cas9 using the immortal JK-1 erythroleukemia line. JK-1 cells spontaneously differentiate, generating cells at different stages of erythropoiesis, including terminally differentiated nucleated RBCs that we term "jkRBCs". A screen of small molecule epigenetic regulators identified several bromodomain-specific inhibitors that promote differentiation, and enable production of synchronous populations of jkRBCs. Global surface proteomic profiling revealed that jkRBCs express all known *P. falciparum* host receptors in a similar fashion to cRBCs and multiple *P. falciparum* strains invade jkRBCs at comparable levels to cRBCs and RBCs. Using CRISPR/Cas9 we deleted two host factors (BSG and CD44) for which no natural nulls exist. BSG interacts with the parasite ligand Rh5, a prominent vaccine candidate. A *BSG* knockout was completely refractory to parasite invasion in a strain-transcendent manner, confirming the essential role for BSG during invasion. CD44 was recently identified in an RNAi screen of blood group genes as a host factor for invasion, and we show that a *CD44* knockout results in strain-transcendent reduction in invasion. Furthermore we demonstrate a functional interaction between these two determinants in mediating *P. falciparum* erythrocyte invasion.

Significance statement (120 words)***:***

During malaria infections, *Plasmodium falciparum* parasites invade red blood cells (RBCs). Identification of host factors for parasite invasion guides the development of vaccines and host-targeted therapeutics. In this work we describe the development of an *in vitro* culture system for the functional analysis of red blood cell determinants using the immortal erythroleukemia cell line JK-1. JK-1 cells can be induced to differentiate synchronously, support parasite invasion and are amenable to genetic manipulation. Using this system we validated two host factors, BSG and CD44, as strain transcendent host factors for parasite invasion and we demonstrated a functional interaction between these two proteins. The ability to perform gene editing to produce RBC mutants will augment our ability to study malaria infection.

Introduction

Malaria is an infectious disease caused by *Plasmodium* parasites and is a major public health burden with upwards of 200 million cases and over 400,000 deaths annually (1). Upon infection of a new host, the parasite replicates in a liver cell following which it establishes a cyclical infection of red blood cells (RBCs), leading to all of the clinical symptoms of disease (2). Invasion of new RBCs occurs rapidly after release of daughter merozoites from mature schizonts (3), and during the invasion process parasites use multiple invasion ligands to bind to the host RBC by interacting with specific host receptors (4-6). Blocking these interactions can lead to a reduction in parasite invasion (7), a strategy underlying blood-stage vaccine design (8, 9).

Fundamental insights into host-parasite interactions during invasion have come from analysis of rare naturally occurring RBC polymorphisms (10) or through biochemical interaction studies using recombinant invasion ligands and recombinant host receptor panels (7, 11). We have focused on a genetic approach, which requires using CD34+ hematopoietic stem cells (HSCs) (12, 13) that allows systematic generation of RBC genetic mutants. Using this system, we have functionally characterized the effects of knockdown of the host receptor GypA on the invasion of the sialic-acid dependent *P. falciparum* strain W2mef (14).

There are several challenges with using primary CD34+ HSCs that include: (i) the short time-frame for introducing gene knockdowns during erythroid differentiation which may limit the extent of knockdown and precludes obtaining clonal cell populations; (ii) primary cell differentiation is terminal leading to the need to repeatedly generate gene knockdowns for each assay; (iii) invasion screening and functional characterization of gene knockdowns requires large numbers of cells which can be costly to generate. The broad range of genetic techniques facilitated byt the the Clustered Regularly Interspaced Short Palindromic Repeats (CRISPR)/Cas9 system (15-19) is highly desirable for modifying RBC host factors to investigate *Plasmodium* invasion, but the use of these techniques remains challenging in primary CD34+ cells (20, 21).

Here we have developed an *in vitro* culture system using the immortal JK-1 erythroleukemia cell (22), that permits the rapid and efficient generation of RBC genetic mutants and overcomes the challenges of using primary CD34+ HSCs. JK-1 cells spontaneously differentiate at low rates to form cells that resemble young, nucleated RBCs. We have developed methods for enriching differentiated cells, and to reduce heterogeneity we screened a library of epigenetic regulators for compounds that induce differentiation. Importantly, the differentiated JK-1 cells support invasion by *P. falciparum*, and combined with the ability to genetically modify the cells provides a platform for the functional characterization of host factors important for parasite invasion. Using this system, we have generated a knockout of the essential host receptor basigin (BSG), for which no natural nulls exist, and which binds the parasite invasion ligand Rh5 (23, 24) now a leading vaccine candidate (9). We show that the *BSG* knockout line is completely refractory for parasite invasion, thus validating BSG as an essential receptor for *P. falciparum* invasion (9, 25).

In a recent shRNA-based forward genetic screen of 42 blood group genes, we identified two host factors important for parasite invasion (CD55 and CD44) (26). CD55 was functionally characterized as an essential host factor for invasion through use of natural CD55 RBC null cells, however similar natural nulls were not available for CD44. Using the JK-1 cell system, we have generated a CD44 knockout and we show that this knockout line displays a pronounced reduction in invasion across multiple parasite strains, confirming the importance of CD44 for *P. falciparum* invasion. As CD44 has been reported to interact with BSG (27-29) we investigated the functional significance of this interaction by using an α-BSG antibody to

inhibit invasion. We find that the *CD44* knockout enhances the α-BSG-dependent inhibition of invasion, indicating a functional interaction between BSG and CD44 during parasite invasion.

Results

JK-1 erythroleukemia cells models erythropoiesis *in vitro*

While *P. falciparum* preferentially invades mature RBCs, it is also capable of invading nucleated RBCs, primarily orthochromatic erythroblasts (14, 26, 30). As such, we were interested in testing the ability of immortal erythroleukemia cell lines to differentiate, form RBCs and support parasite invasion. A search of the literature identified ten different erythroleukemia cell lines that we were able to obtain and culture in the laboratory: Ery-1 (31); K562 (32); KH88/C2F8 (33); B4D6 (33); LAMA-84 (34); TF-1A (35); HEL92.1.7 (36); OCIM (37); OCIM-2 (37); and JK-1 (22) (**Supplementary Figure 1A**). During routine culture, we observed spontaneous differentiation into predominantly polychromatic-like nucleated RBCs (38) in only the JK-1 cell-line. The JK-1 erythroleukemia cell line was isolated from an individual with Philadelphia-chromosome positive chronic myelogenous leukemia and is reported to express HbF (22). A typical JK-1 culture produced a stochastically fluctuating mixture of erythroid-like cells at different sizes and stages of differentiation (**Figure 1**). A majority (>80%) of actively dividing cells was composed of less differentiated proerythroblasts and basophilic erythroblasts. The differentiated nucleated RBCs in the JK-1 cell-line consisted of primarily early- and late-stage polychromatic erythroblasts, with a very small fraction (<1%) of orthochromatic erythroblasts (characterized by fully condensed nuclei (38)) and occasional (<0.5%) enucleated cells (resembling reticulocytes).

Given the heterogeneity of normal JK-1 cell cultures, we tested a number of different techniques to specifically enrich for different cell populations. We observed that cell size varied based on the stage of differentiation with undifferentiated proerythroblasts having almost 2-fold larger diameter than differentiated polychromatic and orthochromatic erythroblasts (**Figure 1A**). We first tested whether we could use fluorescent activated cell sorting (FACS) to separate cells based on size. Using forward scatter (FSC) and side scatter (SSC) parameters, we found a gate that resulted in the enrichment of basophilic, early and late-stage polychromatic cells (small cell gate) and a gate that enriched for proerythroblasts (large cell gate) (**Supplementary Figure 1B**). As FACS is time and resource intensive for sorting large numbers of cells, we next tested whether we could enrich cells using a bulk method. As Percoll density gradients have been used to enrich for hematopoietic cells from bone marrow extracts (39), we tested whether this method would be feasible for JK-1 cells. Centrifuging a mixed population of JK-1 cells through a 52.5% (v/v) Percoll-PBS gradient resulted in an ~15-fold enrichment of differentiated early- and late-stage polychromatic cells in the cell pellet, while proerythroblasts and basophilic erythroblasts were retained at the interface between the Percoll gradient and the culture media (**Figure 1B**). We found that the Percoll-PBS method was faster than FACS and was simple to scale up for large numbers (>10^8) of cells.

Bromodomain inhibition induces differentiation of JK-1 cells

While FACS and Percoll-PBS allowed us to enrich for differentiated jkRBCs, only a relatively small proportion (10 – 15%) of a typical JK-1 culture contained differentiated cells. Therefore we were interested in finding ways of increasing the proportion of differentiated nucleated RBCs in a synchronous manner. We hypothesized that as JK-1 cells display spontaneous differentiation, that this process might be under epigenetic control, and indeed epigenetic regulators have been reported to induce cellular differentiation (40-42). We screened an epigenetic library for small molecule inducers of differentiation. To begin with we required a method of quantitatively monitoring JK-1 differentiation. We observed that

expression of glycophorin A (GypA), a cell surface marker of erythrocyte maturation (43, 44), was correlated with JK-1 differentiation (**Supplementary Figure 2A**). Using a FITC-labelled α-GypA antibody we observed two distinct populations: the GypA-negative fraction (gated based on unstained cells) contained predominantly proerythroblasts and basophilic erythroblasts while the GypA-high fraction was enriched for early- and late-stage polychromatic cells.

Using this method we sorted for a population of GypA-negative JK-1 cells and screened these cells with a library of 96 epigenetic modifiers (Cayman Chemicals, USA). This library includes small molecules that target a wide variety of epigenetic regulatory proteins. Two rounds of screening were performed with cells harvested after 5 days in screen 1 and after both 7 and 14 days in screen 2. Upon harvest, the levels of GypA were measured by flow cytometry and the ratio of GypA-high:GypA-negative was calculated (**Supplementary Figure 2B**). The data from the screen were ranked by hierarchical clustering (**Figure 2A; Supplementary Table 1**). Six compounds were identified that displayed substantial induction of JK-1 cell differentiation. Significantly, four of the six top compounds included inhibitors of bromodomain-containing proteins: two compounds (+)-JQ1 (45) and PFI-1 (46) target mammalian bromodomain and extra terminal domain (BET) proteins; bromosporine is a general bromodomain inhibitor (47); and I-CBP112 targets the bromodomain of cAMP-responsive element-binding protein binding protein (CREBBP)/E1A-associated protein p300 (EP300) (48, 49). The only other bromodomain-specific inhibitor in the library, PFI-3, targets a different category of bromodomain-containing protein (50) and was not found to be an inducer of JK-1 differentiation. The two other top inducers, GSK343 (51) and UNC1999 (52) both target the catalytic core of the polycomb repressive complex 2 (PRC2) enhancer of zeste homologue 2 (EZH2) histone methyltransferase (53).

We validated two top hits, PFI-1 and (+)-JQ1, by testing differentiation with a range of concentrations of compound (**Figure 2B**). In both cases, at high concentrations of compound, cell expansion was inhibited, while at the lowest concentration of compound, cell growth was similar to the DMSO-treated control cells for the first six days following which the cell expansion plateaued. We next monitored cells treated with the optimal concentrations of PFI-1 (2 μM) and (+)-JQ1 (1 μM) during differentiation by staining for GypA and CD34, which is a marker for early hematopoietic stem cells (43) (**Figure 3A**). Both PFI-1 and (+)-JQ1 treatment led to a rapid increase of GypA surface levels resulting in a homogenous population of GypA-positive cells by 8 days post-induction while the un-induced control had a broad mixture of cells with different levels of GypA. CD34 levels also decreased rapidly and were almost undetectable by day 4 in the induced conditions but remained at a low level in the control cells. Analysis of cell morphology (**Figure 3B**) demonstrated that both PFI-1 and (+)-JQ1 treatment resulted in the formation of differentiated cells, whereas the DMSO-treated control cells remained a mixed population. When PFI-1 and (+)-JQ1 are tested in combination (**Supplementary Figure 2C,D**), differentiation is still observed but with reduced cell expansion.

Inhibition with LSD1 inhibitors maintains an undifferentiated state

While the primary focus of the epigenetic screen was to identify compounds that induce synchronous differentiation, we were also interested to see if there were compounds that had the opposite effect. In the screen (**Figure 2A**) we observed a number of compounds that had low levels of differentiation as measured by α-GypA staining. Examination of the flow cytometry data for these compounds over the different days of the assay indicated that the majority of this effect was due to toxicity of the compounds, as the initial GypA-negative population had not expanded. However, we identified one compound, the lysine specific demethylase 1 (LSD1) inhibitor (tranylcypromine), which was able to maintain growth of cells in an undifferentiated state. When a population of GypA-negative cells was treated with

tranylcypromine, the cells grew at the same rate as DMSO-treated control cells, doubling once every ~ 30 hours (**Supplementary Figure 2E**). Tranylcypromine treated cells retained similar levels of GypA, CD34 and CD71 (transferrin receptor) over multiple generations, while DMSO-treated controls showed pronounced increases in GypA levels and reduction of CD34 levels over the same period (**Supplementary Figure 2F**).

JkRBCs functionally resemble nucleated RBCs

Having identified epigenetic factors that could control JK-1 differentiation, we next tested the synchronicity of the differentiated cells. Starting with cells maintained on 10 μM tranylcypromine, we induced differentiation of these cells with 2 μM PFI-1 and between 12 – 14 days post-induction, cells were harvested and passaged through 52.5% (v/v) PBS-Percoll. The resulting cells displayed a high degree of homogeneity and consisted of >90% late-stage polychromatic cells (**Figure 3C**). Next we compared these jkRBCs to bone marrow-derived CD34+ HSCs (cRBCs) and peripheral RBCs. The cRBCs were at day 16 post thaw and consisted of a mixture of cells including basophilic erythroblasts, early- and late-stage polychromatic erythroblasts, orthochromatic erythroblasts, reticulocytes and pyrenocytes (ejected nuclei) (**Supplementary Figure 3A**). Analysis of three independent biological cRBC cultures at 16 – 17-days post-thaw showed that a majority of cells were orthochromatic erythroblasts and reticulocytes (together > 70%), while earlier stage basophilic and polychromatic erythroblasts were present at much lower frequencies (< 10%) (**Supplementary Figure 3B**). A comparison of cell diameter showed that the jkRBCs (**Figure 1A**) were ~ 1.25-fold larger on average than the dominant cRBCs (orthochromatic erythroblasts and reticulocytes). During the process of *P. falciparum* invasion, the parasite interacts with numerous host surface membrane proteins on the surface of peripheral RBCs. In order to check whether jkRBCs expressed known host receptors, we performed flow cytometry to compare the levels of expression of BSG, GypA, GypC, CR1 and CD71 between jkRBCs, cRBCs and peripheral RBCs (**Figure 3D**). The relative flow cytometry signal for three of the known host receptors (GypA, GypC and CR1) were tightly correlated between jkRBCs, cRBCs and peripheral RBCs. The level of BSG was higher in jkRBCs and cRBCs and about 10-fold lower in peripheral RBCs, suggesting that levels of this protein change substantially during the final stages of erythroid maturation. As a control we measured the levels of transferrin receptor (CD71), which is abundant on jkRBCs and cRBCs but is absent from peripheral RBCs, as has been observed previously (54, 55).

We next performed a global analysis of the surface membrane protein composition of jkRBCs by quantitative surface proteomics (26, 56). We identified 237 surface membrane proteins by ≥ 2 peptides, from a total of 677 identified proteins (**Supplementary Table 2**). We compared this dataset to available RBC proteomes (**Supplementary Figure 3C**) and were able to identify 92.2% of the jkRBC proteins in one or more of the published proteomes. The dataset with the greatest overlap (85.9%) included proteomes of not only mature RBCs, but also erythroid progenitors (57). Next we used quantitative surface proteomics to compare the relative abundance of surface membrane proteins between jkRBCs and an equal number of day 16 cRBCs. The relative abundance of a large proportion (68.6%) of the cRBC membrane proteins was within ± 2-fold of the equivalent jkRBC proteins, and 91.1% were within a ± 4-fold range (**Figure 3E**). A comparison of the blood group proteins (**Supplementary Figure 3D**) showed a similar pattern. The majority of proteins, including known *P. falciparum* host receptors GypA, GypC, CR1 and BSG, were within a 2-fold range. By this method, we are not able to distinguish GypA and GypB, so the signal we observe for GypA is a combination of GypA and GypB. We also identified three proteins with greater than 4-fold abundance (BCAM, CD99, SLC14A1) in cRBCs compared to jkRBCs.

JkRBCs support invasion by *P. falciparum*

We next tested the ability of jkRBCs to support *P. falciparum* invasion as has been observed for other nucleated erythroid precursors (14, 30, 58). Indeed we observed invasion into jkRBCs by two different strains of *P. falciparum*: the sialic acid-independent strain 3D7 (59) and the sialic acid-dependent strain Dd2 (60) (**Figure 4A**). To compare invasion efficiency of *P. falciparum* into jkRBCs, cRBCs and RBCs we measured the parasitized erythrocyte multiplication rate (PEMR) (% final ring parasitemia/% initial schizontemia) between the different cell types. The invasion rates of *P. falciparum* strains 3D7 and Dd2 into jkRBCs were comparable to invasion into cRBCs and RBCs (**Figure 4B)**, suggesting that jkRBCs express sufficient levels of all relevant host receptors and possess the requisite glycosylation required for parasite binding and invasion (4, 6). Since we often observed multiple parasites invading into a single host jkRBC, we quantified the preference for multiple parasite invasion events by determining the selectivity index (SI) (61) (**Supplementary Figure 3E)**. The SI is a measure of the observed number of multiply-infected cells compared to the number expected by chance based on a Poisson distribution, and can be used to determine the susceptibility of host cells to invasion by *Plasmodium* parasites. The jkRBCs showed the highest SI followed by cRBCs and RBCs. To determine whether *P. falciparum* parasites grew normally in jkRBCs, we assessed parasite growth during a single cycle (**Supplementary Figure 4**). While parasites were occasionally observed to develop into trophozoites and schizonts, development of these stages was significantly impeded compared to RBCs.

Generation of a BSG knockout via CRISPR/Cas9

We next tested if it was possible to genetically manipulate the JK-1 cells. We transduced the JK-1 cells with a lentivirus expressing an shRNA targeting *GYPA* and monitored protein levels by flow cytometry. We were able to detect a substantial decrease in GypA protein expression within about 1 week post-transduction (**Supplementary Figure 5A**) thus confirming that shRNA gene knockdowns were supported by JK-1 cells. We then attempted to generate gene knockouts using the CRISPR/Cas9 gene editing system (19) (**Supplementary Figure 5B**). We chose the human *BSG* gene encoding the basigin receptor (Ok blood group (62)), which is an essential receptor for *P. falciparum* (7). We first generated lentivirus containing the LentiCas9-Blast plasmid (19) and introduced it by viral transduction into JK-1 cells. Cells were selected by growth on blasticidin until a stable JK-1-Cas9 cell line was obtained. No toxicity or difference in growth rate associated with Cas9 expression was observed. Next, three single-guide RNAs (sgRNAs) targeting *BSG* were individually cloned into the LentiGuide-Puro vector (19) and these constructs were virally transduced into the LentiCas9-positive JK-1 cells. After 2 – 4 weeks of selection, single cell clones were obtained by limiting dilution of the bulk population. The presence of gene knockouts in these clonal cell lines was assessed by loss of α-BSG flow cytometry staining and subsequently verified by Sanger sequencing and Tracking of Indels by Decomposition (TIDE) analysis (**Supplementary Figure 5C-E**). Of the three sgRNAs we tested, we only observed one single-guide that showed a complete loss of α-BSG flow staining in the bulk population (BSG-1 sgRNA), and following cloning two individual clonal lines were obtained (*ΔBGS-1* and *ΔBSG-2*) from this sgRNA, both with different deletions in each gene copy (**Supplementary Figure 5C,D**). The BSG-1 sgRNA targeted the N-terminus of the BSG protein and the resulting deletions disrupted the initiator methionine ATG codon (**Supplementary Figure 5E**).

In order to validate the *BSG* knockout jkRBCs did not have any RBC developmental defects, we compared the expression levels of BSG, GypA, GypC and CR1 by flow cytometry for JK-1 wildtype and *ΔBSG* jkRBCs (**Figure 5A**). The *ΔBSG* cells showed a complete loss of α-BSG signal, confirming a functional loss of BSG protein. The levels of GypA, GpyC and CR1 were very similar between the WT and *ΔBSG* lines. To further confirm that deletion of *BSG* did not result in changes to any other surface membrane protein, we compared the abundance of surface proteins from Δ*BSG* jkRBCs to wild type jkRBCs using quantitative

surface proteomics (**Figure 5B, Supplementary Table 2**). Our data demonstrate that the knockout of *BSG* was specific and did not lead to the significant alteration of other surface membrane proteins.

BSG is essential for *P. falciparum* invasion

Basigin is proposed to be an essential receptor for *P. falciparum* (7) and we have previously demonstrated that knockdown of *BSG* in CD34+ HSCs via shRNA leads to a substantial decrease (~80%) in invasion by multiple strains of *P. falciparum* (7). While there is strong evidence that *BSG* is an essential receptor for *P. falciparum*, the residual invasion observed with the *BSG* knockdown (7) raised some doubts about whether loss of *BSG* would completely block *P. falciparum* invasion. There are natural *BSG* polymorphisms that occur as part of the Ok blood group (62), but to date no natural *BSG* nulls have been described. To determine the effect of deleting *BSG* in jkRBCs, we performed invasion assays with two different strains of *P. falciparum* (3D7 and Dd2) using two independent *BSG* knockout clones (Δ*BSG*-1 and Δ*BSG*-2), both generated using the BSG-1 sgRNA. We observed a complete inhibition of invasion into both Δ*BSG* clones for both *P. falciparum* strains (**Figure 5C**). This result provides strong evidence that BSG is required for strain-transcendent invasion.

CD44 is a strain-transcendent invasion host factor

CD44 was identified as a potential host receptor during a screen of blood group gene knockdowns (26). Knockdowns of CD44 in CD34+ HSCs led to a modest reduction in *P. falciparum* invasion, but this was only tested in the 3D7 strain and functional characterization of CD44 was limited by the lack of naturally occurring CD44 nulls. Therefore, we generated a knockout of *CD44* using CRISPR/Cas9 and we obtained mutant cells with an insertion in the exon 2 that leads to the formation of a premature stop codon and truncation of the protein in the N-terminal extracellular domain (**Supplementary Figure 6A,B**). We confirmed the knockout of *CD44* was specific by flow cytometry (**Supplementary Figure 6C**) and quantitative surface proteomics (**Figure 6A**) where we did not observe a significant change in abundance specifically of any known host receptor (BSG, GypA, GypC, CR1) or other surface membrane protein. We next tested invasion of multiple *P. falciparum* strains into two *CD44* knockout clonal lines (ΔCD44-1 and ΔCD44-2) and we observed a consistent inhibition of invasion (between ~ 30 – 40%) across multiple parasite strains including the sialic acid independent 3D7 and sialic acid dependent W2mef strains (**Figure 6B**), confirming the importance of CD44 in *P. falciparum* invasion.

CD44 functionally interacts with BSG

CD44 has been reported to interact with BSG in multiple cancer cell lines (27-29) prompting us to test whether there was a functional interaction between CD44 and BSG. To do so, we used the monoclonal MEM6/6 α-BSG antibody, which has previously been shown to inhibit parasite invasion (7), to inhibit *P. falciparum* 3D7 invasion into JK-1 wild type and ΔCD44-1 cells (**Figure 6C**). We observed an approximately 2-fold reduction in IC_{50} for the Δ*CD44*-1 knockouts compared to WT JK-1 cells, indicating that the Δ*CD44*-1 knockout cells were more sensitive to inhibition by the α-BSG antibody. We next checked if this could be explained by differences in levels of BSG on JK-1 WT and Δ*CD44*-1 knockout cells. However, we did not observe any significant difference in BSG protein levels either by flow cytometry (**Supplementary Figure 6D**) or by quantitative surface proteomics (**Supplementary Table 2**). Next we tested the effect of inhibition of an invasion step downstream of Rh5/BSG by using the R1 peptide that inhibits the interaction between the parasite factors AMA1 and RON2, which are involved in strong attachment of the invading merozoite (**Figure 6D**) (63, 64). In this case we observed an approximately 2-fold increase in IC_{50} in the Δ*CD44*-1

knockout compared to the JK-1 WT, indicating an increased utilization of the AMA1/RON2 interaction in the absence of CD44.

Discussion

A major area of interest in *Plasmodium* biology has been the identification of essential, strain transcendent host receptors since their cognate invasion ligands may be potent vaccine candidates (9). We have developed an *in vitro* culture system for functional analysis of the host contribution to blood-stage *Plasmodium falciparum* invasion using the JK-1 erythroleukemia cell line, which displayed unique features: (i) JK-1 cells naturally produced erythroid lineage cells (proerythroblast-, basophilic-, polychromatic- and orthochromatic-like cells) and using small-molecule epigenetic modifiers, we were able to either maintain the cells in an undifferentiated state or to predictably induce synchronous differentiation to produce jkRBCs (nucleated RBCs). (ii) JkRBCs functionally resembled differentiated cRBCs and peripheral RBCs. The surface membrane protein composition of jkRBCs was comparable in composition to cRBCs and peripheral RBCs, and known *P. falciparum* host receptors were expressed at levels equal to or greater than RBCs and cRBCs. Critically, jkRBCs supported robust invasion of multiple *P. falciparum* strains, implying the presence of all the requisite host factors were at sufficient levels for parasite invasion. (iii) JK-1 cells were readily amenable to different genetic modifications such as gene knockdowns via RNAi and gene knockouts via CRISPR/Cas9, which have been challenging in primary CD34+ HSCs (20, 21). (iv) As JK-1 cells are immortal, we were able to generate clonal mutant cell lines and were able to freeze down, thaw and cost-effectively produce large numbers of wild type and mutant cells.

In our screen for epigenetic factors that induce synchronous differentiation of JK-1 cells, the most potent inducers targeted bromodomain-containing proteins. Bromodomain proteins bind to acetylated ε-amino lysine residues on histones and are involved in the regulation of gene expression (65, 66). The two top inducers of JK-1 differentiation, (+)-JQ1 and PFI-1, despite having different chemical scaffolds, target BET family proteins which consists of four members: BRD2, BRD3, BRD4 and BRDT (67, 68). BET family proteins are involved in multiple transcription complexes and help regulate cell growth (69). In the context of erythropoiesis, they promote chromatin occupancy of acetylated forms of the global erythroid transcription factor GATA-1 (70, 71) which itself modulates gene expression during erythropoiesis. With the ability to genetically manipulate JK-1 cells, it may be possible to elicit controlled induction of differentiation independent of epigenetic regulators, by directly controlling levels of BET protein expression, e.g. by knock-in of destabilization domain tags (72).

The composition of the surface membrane proteome of jkRBCs shares a high degree of overlap with published RBC proteomes. Our quantitative surface proteomics analysis comparing cRBCs and jkRBCs showed that >90% of proteins were expressed within a 4-fold range. Instances of higher protein abundance on jkRBCs compared to cRBCs and RBCs (e.g. BSG) may be explained by: (i) the overall larger size of jkRBCs compared to cRBCs and RBCs; (ii) the greater homogeneity and relative immaturity of jkRBCs (late-stage polychromatic cells) compared to cRBCs (orthochromatic cells and reticulocytes); (iii) and the overall decrease in protein abundance per cell during erythropoiesis (57). While we observed variation in the levels of surface membrane proteins, jkRBCs supported equivalent *P. falciparum* invasion rates as cRBCs, indicating that none of the essential host receptors is limiting. However it is possible that the variation in surface membrane protein levels may result in differences in invasion between jkRBCs and cRBCs/peripheral RBCs when host receptor levels are modified (e.g. by enzyme treatment or by knockout of non-essential receptors~~).~~

One limitation of jkRBCs is the relative immaturity of these cells compared to cRBCs, as judged by the larger average size, higher levels of CD71 and deficiency in forming reticulocytes. These features likely stem from the cancer-causing mutations (22) that favor continued cell replication instead of terminal differentiation. JK-1 cells have double Philadelphia chromosomes, which is typically linked with the formation of the BCR-ABL kinase oncogene (73). The relative immaturity of jkRBCs and the expression of HbF (22) may explain the delayed growth of *P. falciparum* post-invasion. A similar effect has been observed with parasite invasion into younger CD34+ basophilic and polychromatic erythroblasts (30). In order to study parasite growth we could either (i) screen for genetic mutations in JK-1 cells that support parasite growth and/or (ii) adapt parasites to growth in JK-1 cells by long-term propagation as has been shown for *P. knowlesi* adaptation to growth in human reticulocytes (74).

The JK-1 cell culture system has facilitated functional characterization of two host factors (BSG and CD44) important in *P. falciparum* invasion. *BSG* null cells have not been found naturally and strain-transcendent inhibition with BSG was demonstrated using anti-BSG or anti-RH5 antibodies, often at high concentrations (7, 25, 75). We have previously generated a *BSG* knockdown by RNAi in CD34+ HSCs, which showed ~ 80% reduction in invasion efficiency (7). We hypothesized that the remaining invasion could be due to residual BSG protein present on the knockdown cells. Using the JK-1 system and CRISPR/Cas9 to generate Δ*BSG* cell lines has allowed us to confirm that the loss of BSG expression results in complete inhibition of invasion of multiple parasite strains, thus confirming the essential role that BSG plays in parasite invasion.

CD44 was identified as an invasion host factor in a forward genetic RNAi screen of blood group genes (26), but its role in invasion could not be fully characterized due to the absence of natural *CD44* null cells. We observed that knockout of *CD44* resulted in consistent reduction of invasion efficiency, in a strain-transcendent fashion, confirming the importance of CD44 as a host factor for *P. falciparum* invasion. Furthermore, we observed a functional interaction between CD44 and BSG, as measured by a reduction in IC_{50} of the α-BSG MEM6/6 antibody in Δ*CD44*-1 knockout cells compared to JK-1 WT. This effect is not simply due to decreased levels of BSG in the Δ*CD44*-1 knockout cells. Other possible explanations include CD44 functioning either directly as a host receptor at an earlier stage than the Rh5/BSG interaction (76) – in this case loss of CD44 would result in reduced number of parasites successfully reaching the Rh5/BSG step of invasion. Alternatively, based on the reported CD44/BSG interaction (27-29), CD44 could be operating directly as a co-receptor with BSG and could be prompting the parasite to preferentially utilize a subset of BSG bound to CD44 during invasion.

In contrast to the effect of inhibition of Rh5/BSG, we observed an increase in IC_{50} of the R1 peptide inhibition of AMA1/RON2 in the Δ*CD44* knockout compared to the JK-1 WT. AMA1 and RON2 are parasite-derived factors that are host receptor independent and mediate strong attachment of the merozoite (63, 64) at a step downstream of the Rh5/BSG interaction (76). Similar antagonistic effects of inhibition of Rh5/BSG and AMA1/RON2 have been reported previously (77, 78). As the *CD44* knockout is synergistic with BSG inhibition, and as AMA1 and RON2 are parasite-derived, we suggest that the CD44 function maps with BSG rather than AMA1/RON2. Therefore, one possible consequence of loss of CD44 (based on the limited-area model for invasion-ligand/host-receptor interactions (79)) may be the reduced engagement of an earlier invasion ligand (e.g. Rh5). As such there would be a subsequent increase in the available space for AMA1/RON2 at the apical end of the merozoite during RBC attachment (77, 79), thus resulting in an increased utilization of the AMA1/RON2 pathway. Of great interest with regards the function of CD44 during invasion include the identification of any potential parasite invasion ligand, the effect of previously reported CD44 interaction with cytoskeletal proteins band 4.1 and ankyrin (80) and possible signaling roles of CD44 during invasion, either separately or in parallel with BSG (81).

The versatility of the JK-1 *in vitro* culture system in supporting both robust parasite invasion and simple genetic manipulation to produce gene knockouts will facilitate the functional analysis of the host contribution to *P. falciparum* invasion. Indeed, the identification and characterization of essential and strain-transcendent host factors and the parasite molecules with which they interact is a vital aspect of understanding parasite invasion biology and will ultimately aid in the development of vaccines and host-targeted therapeutics.

Materials and Methods

Cell culture

The following eythroleukemia cell lines were obtained from the Leibniz Institute DSMZ-German Collection of Microorganisms and Cell Cultures: JK-1 (catalogue #ACC347), OCIM-1 (ACC529), OCIM-2 (ACC619) and LAMA84 (ACC168). The following erythroleukemia cell lines were obtained from the American Type Culture Collection: HEL 92.1.7 (TIB-180), K562 (CCL-243) and TF-1A (CRL-2451). The C2F8 and B4D6 cell lines were kind gifts of Dr. Tatsuo Furukawa (Niigata University School of Medicine, Japan) (33). The Ery-1 cell line was a kind gift of Dr. Michael Arock (Unité CNRS UMR 8147, Paris, France) (31). The erythroleukemia cell lines were propagated in Iscove's Modified Dulbecco's Medium (IMDM) with Glutamax (Thermo Fisher Scientific) and supplemented with 0.5% (v/v) penicillin/streptomycin (Thermo Fisher Scientific) and either 10% AB+ heat-inactivated serum (Interstate Blood Bank) or 10% AB+ octaplas®LG (OctoPharma) with 2 IU/mL heparin (Affymetrix). Cells were maintained at between 1 x 10^5/mL to 1 x 10^6/mL in vented T-flasks (BDFalcon) at 37°C in a humidified chamber with 5% (v/v) CO_2. When necessary, cells were frozen in growth media + 5% (v/v) dimethylsulfoxide (Sigma-Aldrich). JK-1 clones were obtained by limiting dilution and all subsequent experiments were performed with the JK-1-7B clone. CD34+ hematopoietic stem cells (Lonza) were cultured as described previously (12, 13, 26). Cytospins were prepared as described previously (26) and stained with May-Grünwald (Sigma-Aldrich) followed by Giemsa (Sigma-Aldrich) according to the manufacturer's instructions. A double-chamber Neubauer hemocytometer (VWR) was used for live cell counting.

Percoll density gradients

The Percoll (GE Healthcare) density gradients were prepared based on modifications to an existing protocol (39), by mixing stock Percoll (100%) to the indicated final volumetric dilution (e.g. 52.5% (v/v)) with 1 volume of 10X PBS (final concentration 1X) and the remainder with ddH_2O. The pH was adjusted to 7.40 with HCl, following which the mixture was filtered through a 0.2 µm sterile filter (Millipore). Typically 4 mL of the gradients were added to a 15 mL Falcon tube and a suspension of cells in 4 mL IMDM + 10% AB+ media were gently layered on top of the Percoll cushion. The cells were pelleted at 500 *g* for 10 minutes with low acceleration and low braking. Following the centrifugation, the interface and pellet fractions were transferred to separate 15 mL Falcon tubes and washed 2x with IMDM.

Flow cytometry and fluorescent activated cell sorting

For flow cytometry, between 1 – 5 x 10^5 cells were washed into flow buffer (PBS + 0.5% (w/v) BSA) and allowed to bind to antibodies for 30 minutes at room temperature and protected from light. The following antibodies and dilutions were used: 1 in 200 AlexaFluor 647 goat-α-mouse (Thermo Fisher Scientific); 1 in 100 α-BSG-FITC (ThermoFisher Scientific); 1 in 20 α-CD34-FITC (Miltenyi Biotech); 1 in 20 α-CD71-APC (Miltenyi Biotech); 1 in 100 α-CR1 (Santa Cruz Biotechnology); 1 in 100 α-GypA-FITC (StemCell Technologies); 1 in 2000 α-GypC-FITC (Santa Cruz Biotechnology); 1 in 20 α-CD44-APC (Miltenyi Biotech). Samples were washed in flow buffer and analyzed on a Milteny MACSQuant instrument equipped with 405 nm, 488 nm and 638 nm lasers and an autosampler. During flow cytometry measurements, cells were stained with propidium iodide (Miltenyi Biotec, San Diego, CA) to exclude live/dead cells. Flow cytometry data were analyzed using *FlowJo* v 10.2. For FACS analysis, cells were sorted on a BioRad S3 cell sorter equipped with both 488 nm and 561 nm lasers.

Epigenetic library screening

A focused library of 96 epigenetic modifiers (Cayman Chemicals) was screened for the ability to induce differentiation of JK-1 cells. Undifferentiated JK-1 cells were obtained by FACS by gating for an α-GypA-FITC-negative population. In the first experimental run, cells were diluted to 4.0 x 10^4 cells/well in 200 µL

JK-1 growth media in 96-well flat-bottom plates (Falcon) and epigenetic modifiers were added to 10 µM or 1 µM final concentration using the robotics facility at the Institute of Chemistry and Cell Biology at Harvard Medical School. Cells were grown for 5 days under standard growth conditions prior to harvesting. In the second experimental run, cells were diluted to 8.0 x 10^3 cells/well with the same two concentrations of epigenetic modifiers (10 µM and 1 µM). Half of the cells were harvested 7-days post setup and the media was refreshed for the remainder of the cells which were allowed to grow until 14-days post setup. The harvested cells were stained with α-GypA-FITC and the level of GypA was measured by flow cytometry on a Miltenyi MACSQuant (Miltenyi). The ratio of GypA-high:GypA-negative was calculated from plots of SSC vs α-GypA-FITC (see **Supplementary Figure 2A,B**) for each compound and the values were normalized to the highest ratio for each concentration of each experimental run. The data were clustered using *Gene Cluster v3.0* (82) by hierarchical clustering with a Euclidean distance similarity metric and complete linkage. The data were visualized using *TreeView v1.1.6r4* (83).

Cloning and Lentivirus Generation

GuideRNA target sequences were identified bioinformatically using the Broad Institute Genetic Perturbation Platform sgRNA designer tool (https://portals.broadinstitute.org/gpp/public/analysis-tools/sgrna-design) (84). Primers for the top three hits for BSG and CD44 were synthesized (Integrated DNA Technologies, Coralville, Iowa): BSG-1-F 5′-CACCGGCGAGGAATAGGAATCATGG; BSG-1-RC 5′-AAACCCATGATTCCTATTCCTCGCC; BSG-2-F 5′-CACCGTCTTCATCTACGAGAAGCGC; BSG-2-RC 5′-AAACGCGCTTCTCGTAGATGAAGAC; BSG-3-F 5′- CACCGCGTTGCACCGGTACTGGCCG; BSG-3-RC 5′-AAACCGGCCAGTACCGGTGCAACGC; CD44-1-F 5′- CACCGCGTGGAATACACCTGCAAAG; CD44-1-RC 5′-AAACCTTTGCAGGTGTATTCCACGC; CD44-2-F 5′- CACCGACTGATGATGACGTGAGCAG; CD44-2-RC 5′-AAACCTGCTCACGTCATCATCAGTC; CD44-3-F 5′-CACCGCTGTGCAGCAAACAACACAG; CD44-3-RC 5′-AAACCTGTGTTGTTTGCTGCACAGC. Primer pairs were phosphorylated using T4 polynucleotide kinase (New England Biolabs) and ligated using Quick Ligase (New England Biolabs) into the LentiGuide-Puro vector (19), which had previously been digested with *BsmB*I (Thermo Fisher Scientific) and dephosphorylated with FastAP alkaline phosphatase (Thermo Fisher Scientific). Ligated plasmids were transformed into Stbl3 bacteria (Thermo Fisher Scientific) and selected with 100 µg/mL carbenicillin on Luria-Bertani agar plates. Correctly-integrated sgRNAs were confirmed by Sanger sequencing using the U6 promoter: 5′-GACTATCATATGCTTACCGT (19). Plasmid DNA was purified using MaxiPreps (Qiagen) and used to generate lentivirus using established protocols (85)

CRISPR/Cas9 knockouts

CRISPR/Cas9 knockouts were generated following existing protocols (17, 19). First JK-1 cells were transduced with the LentiCRISPR-Blast vector and selected with 6 µg/mL blasticidin (Sigma-Aldrich). The basticidin-resistant cells were next transduced with the LentiGuide-Puro vectors containing each of the three *BSG* sgRNAs and cells were selected for by growing with both 6 µg/mL blasticidin and 2 µg/mL puromycin (Sigma-Aldrich). Knockout generation were monitored by flow cytometry and once cultures had >50% knockout cells, the population was cloned by limiting dilution. Of the 3 sgRNAs tested only BSG-1 resulted in generation of *BSG* knockouts. Individual clones were screened by Sanger sequencing using the following primer sets: BSG-1-seq-F 5′- AAGCAGGAAGGAAGAAATG; BSG-1-seq-RC 5′-TTCACGCCCACACACAGAG followed by TIDE analysis (86) to find bi-allelic knockouts. For CD44, of the 3 tested sgRNAs, only CD44-1 Resulted in generation of *CD44* knockouts. The DNA region around the target site was PCR amplified using the following primers, CD44-1-seq-F 5′-AGCGAATTCTGGGATTGTAGGCATGAG and CD44-1-seq-RC 5′-TGTCTAGAGGTGCTGGTCTCTTACCTG, digested with EcoRI (NEB) and XbaI (NEB), ligated into a carrier plasmid and transformed into XL-10 Gold cells (Agilent) to obtain bacterial clones. The DNA sequence around the sgRNA cut site was subsequently obtained by Sanger sequencing.

Quantitative Surface Proteomics

Plasma membrane profiling was performed as described (56, 87) using 2 x 10^7 of two batches of wild-type jkRBCs, one batch each of the two different Δ*BSG* clones, one batch each of the two different CD44 clones and one batch of day 16 CD34+ cRBCs. Surface membrane proteins were identified following labeling of sialic acid residues with aminooxy-biotin and after processing and generation of tryptic peptides, these were labeled with isobaric tandem mass tags (56) in a 1:1:1:1:1:1:1 ratio. These labeled peptides were enriched and subjected to mass spectrometry as described in supplementary methods.

Invasion assays

All parasite assays were performed with either *P. falciparum* 3D7 attB::TdTomato or *P. falciparum* Dd2 attB::TdTomato strains unless otherwise indicated (see Supplementary Materials for description of these lines). Parasites were cultured following established protocols (88, 89) at 2% hematocrit in O+ blood (Interstate Blood Bank) in complete RPMI media with 0.5% (w/v) albumax and 0.2% (w/v) sodium bicarbonate at 37°C with 5% (v/v) CO_2 and 1% (v/v) O_2. Invasion assays were performed as described (14, 26, 77). Typically invasion assays were prepared with 0.5 – 1.5 x 10^6 cells in 50 µL complete IMDM media in a half-area 96-well plate (Corning) with between 0.5 – 2.0% schizonts (enriched by magnetic LD columns (Miltenyi Biotec) (90, 91)). Cytospins were prepared immediately upon mixing the schizonts and target cells as well as 18 – 24 hours post invasion. Slides were stained with May-Grünwald-Giemsa as described and parasitemia was evaluated by reticle counting (92, 93). For invasion inhibition assays, the MEM6/6 clone of the α-BSG antibody (preservative free) was used (Invitrogen) along with a matched isotype control antibody (preservative free) (Invitrogen). R1 peptide (63, 64) was prepared in complete RPMI media with 0.5% (w/v) albumax and 0.2% (w/v) sodium bicarbonate.

Acknowledgements

The *P. falciparum* 3D7*attB* and Dd2*attB* parasite lines were a kind gift from Prof. David Fidock (Department of Microbiology & Immunology, Columbia University, New York, NY, USA). The TdTomato plasmid was a kind gift from Prof. Matthias Marti (Institute of Infection, Immunity and Inflammation, University of Glasgow, Scotland, UK). The LentiCas9-Blast and LentiGuide-Puro vectors were gifts from John Doench and David Root (Broad Institute, Cambridge, MA, USA). We thank James Williamson (Cambridge Institute for Medical Research, Cambridge, UK) for assistance with mass spectrometry. We thank Stewart Rudnicki and Katrina Rudnicki (Institute of Chemistry and Cell Biology at Harvard Medical School, Boston, MA) for assistance with preparing the chemical library for screening. UK was supported by a Canadian Institutes of Health Research Postdoctoral Fellowship. CG was supported by a Swiss National Science Foundation Postdoctoral Fellowship. MPW was supported by a Wellcome Trust Senior Clinical Research Fellowship (108070/Z/15/Z). This work was supported by a National Institutes of Health R01 grant (R01AI091787 and R01HL139337 to MTD) and by a Bill and Melinda Gates Foundation Grant (OPP1023594, MTD).

Figure Legends

Figure 1. JK-1 erythroleukemia cell line models erythropoeisis, and homogenous populations of differentiated cells can be obtained by density sedimentation and FACS. (**A**) Cells at different stages of differentiation including proerythroblasts, basophilic erythroblasts, polychromatic erythroblasts (early and late) and orthochromatic erythroblasts (38, 94) were observed in a typical JK-1 cell culture. The dimensions of 50 - 100 cells of each of the stages was measured from stained images using *Photoshop* v. 13.0. For each cell a measurement was made of both the longest (D1) and shortest (D2) diameter and the average (also indicated numerically) and standard deviation for each range are shown. (**B**) Layering of a mixed population of JK-1 cells on a 52.5% (v/v) Percoll-PBS gradient leads to the enrichment of early and late-stage polychromatic cells in the pellet fraction and retention of undifferentiated proerythroblast and basophilic cells at the interface. For all images, cells were stained with May-Grünwald-Giemsa and scale bars represent 10 µm.

Figure 2. Screen of epigenetic library to identify inducers of JK-1 differentiation. (**A**) Heat-map showing the results of epigenetic screen for inducers of JK-1 differentiation. The signals have been normalized to the DMSO control (black arrow). Of the top 6 inducers (red bar), four of the compounds target bromodomain-containing proteins indicating a possible conserved mechanism of induction of differentiation. The full list of the 96-epigenetic modifiers is provided in **Supplementary Table 1**. (**B**) Validation of two of the top hits from the epigenetic screen (PFI-1 and (+)-JQ1) showing the fold expansion of undifferentiated JK-1 cells at different concentrations of compounds. Data shown are averages and standard deviations from three technical replicates from a representative biological assay.

Figure 3. Generation of synchronous jkRBCs and comparison with cRBCs and peripheral RBCs. (**A**) Flow cytometry plots showing changes in expression of GypA and CD34 during differentiation for DMSO control treated cells, cells treated with 2.0 µM PFI-1 or 1.0 µM (+)-JQ1. (**B**) Representative microscopy images of differentiating cells stained with May-Grünwald-Giemsa. Scale bar on all images is 10 µm. (**C**) Demonstration of the homogeneity of induced JK-1 cells at 12 – 14 days post-induction with 2 µM PFI-1 and post passage through 52.5% (v/v) PBS-Percoll gradients. Average and standard deviation from 10 independent inductions are shown, with counts from at least 1000 cells per experiment. (**D**) Comparison of jkRBCs, day 16 cRBCs and peripheral RBCs. Representative microscopy images are shown alongside flow cytometry plots measuring the expression of known host receptors BSG, GypA, GypC, CR1 as well as the immature erythroid cell marker CD71. (**E**) The relative abundance of the 237 surface membrane proteins identified by quantitative surface proteomics was compared between jkRBCs and day 16 cRBCs. P values were estimated using Benjamini-Hochberg corrected significance A values as previously described for this approach (56, 87, 95) and proteins with highly significant fold change are indicated.

Figure 4. JkRBCs support invasion of multiple strains of *P. falciparum* at levels comparable to cRBCs and RBCs. (**A**) Representative images of *P. falciparum* 3D7 and Dd2 parasites after successful invasion into jkRBCs. Scale bar on all images is 10 µm. (**B**) Parasitized erythrocyte multiplication rate (PEMR) values (% final ring parasitemia/% initial schizontemia) for *P. falciparum* 3D7 and Dd2 strains were similar between jkRBCs, cRBCs and RBCs. Average and standard deviation are from four biological replicates.

Figure 5. Use of CRISPR/Cas9 to generate *BSG* knockout in JK-1 cells. (**A**) The ΔBSG clone has no surface expression of BSG but retains expression of known host receptors (GypA, GypC and CR1) at levels comparable to jkRBCs. Scale bar on all images is 10 µm. (**B**) Quantitative surface proteomics analysis comparing abundance of 237 surface membrane proteins between WT jkRBCs and ΔBSG jkRBCs confirm the specific loss of BSG in the ΔBSG cells. (**C**) ΔBSG knockout JK-1 cell line is refractory to *P. falciparum*

Invasion. Invasion of the sialic acid independent *P. falciparum* strain 3D7 and sialic acid dependent *P. falciparum* strain Dd2 was completely inhibited in two independent clones of ΔBSG. Data are normalized to invasion efficiency of wild type JK-1 cells and are representative of three biological replicates. Error bars represent standard deviations from 3 biological replicates. P values were calculated using a two-tailed T test (*GraphPad Prism* version 7.01).

Figure 6. CD44 knockout results in a strain-transcendent reduction in parasite invasion. **(A)** Quantitative surface proteomics analysis confirming that the loss of CD44 in the ΔCD44 clone is specific. **(B)** Comparison of invasion efficiency between wild-type and two ΔCD44 knockout clones with multiple *P. falciparum* strains demonstrates a consistent reduction in invasion efficiency. Data for each parasite strain are normalized to invasion efficiency of wild-type JK-1 cells and are representative of between 2 – 3 biological replicates. Error bars represent standard deviations and *P* values were calculated using a two-tailed T test (*GraphPad Prism* version 7.01). **(C)** The ΔCD44 knockout has a reduced sensitivity to inhibition of invasion using the MEM6/6 α-BSG antibody suggesting a functional interaction between BSG and CD44 during parasite invasion. Data were normalized to invasion efficiency of the isotype controls and a representative plot is shown where error bars represent the standard deviation from three technical replicates. **(D)** Inhibition of invasion via dilution series of R1 peptide shows that the ΔCD44 knockout has a greater resistance to inhibition compared to the JK-1 wild type. A representative plot is shown with error bars representing standard deviation from three technical replicates. For both **(C)** and **(D)**, IC_{50} values were calculated using a least-squares fit with log(inhibitor) vs normalized response and a variable slope using *GraphPad Prism* version 7.01. Below the plots, the average IC50 values for JK-1 and ΔCD44 are shown for three biological replicates (α-BSG, **C**) or four biological replicates (R1 peptide, **D**) with the standard error of the mean indicated in brackets. A paired, two-tailed T-test was used to calculate the *P*-value.

Supplementary Material

Parasite cell line generation

The tdTomato sequence was amplified from a plasmid containing the tdTomato coding sequence (96) using the following primers: pCG110-F 5'-AGTACCTAGGATGGTGAGCAAGGGCGAG and pCG111-RC 5'-AGTACTCGAGTTACTTGTACAGCTCGTCCATGC. The PCR product was digested with AvrII and XhoI (New England Biolabs) and cloned into pEcDamHI (97). For transfection, 100 µg of tdTomato containing plasmid were co-transfected with plasmid pINT into 3D7*attB* and Dd2*attB* parasites as described previously (98). Cultures were selected with G418 (125 µg/ml for Dd2 and 250 µg/ml for 3D7), 2.5 µg/ml blasticidin and 2.5 nM WR99210 for 7 days after transfection followed by continuous selection with blasticidin and WR99210 alone.

Generation of JK-1 shRNA knockdowns

Lentivirus of the pLKO plasmid containing the shRNA against *GYPA* (TRCN0000116455) was obtained from the Broad Institute, Cambridge, MA. Lentiviral transduction into JK-1 cells was performed based on existing protocols used for CD34+ hematopoietic stem cells (14, 26).

Quantitative Surface Proteomics

The quantitative surface proteomics is based on previously described methods (56, 87). Briefly, 2×10^7 of each cell type were washed with PBS. Surface sialic acid residues were oxidized with sodium meta-periodate (Thermo Fisher Scientific) then biotinylated with aminooxy-biotin (Biotium). The reaction was quenched, and the biotinylated cells incubated in a 1% Triton X-100 lysis buffer. Biotinylated glycoproteins were enriched with high affinity streptavidin agarose beads (Pierce) and washed extensively. Captured protein was denatured with dithiotreitol (SigmaAldrich), alkylated with iodoacetamide (IAA, Sigma) and digested on-bead with trypsin (Promega) in 200 mM HEPES pH 8.5 for 3 hours. Tryptic peptides were collected and labeled using TMT reagents (56). The reaction was quenched with hydroxylamine, and TMT-labeled samples combined in a 1:1:1:1:1:1:1 ratio. Labeled peptides were enriched and desalted following which 75% of the total sample was separated into six fractions using tip-based strong cation exchange as previously described (56), and 10% of the total sample was subjected to mass spectrometry unfractionated.

Mass spectrometry data was acquired using an Orbitrap Fusion coupled with an UltiMate 3000 Nano LC (Thermo Fisher Scientific, San Jose, CA). Peptides were separated on a 75 cm PepMap C18 column (Thermo Fisher Scientific). Peptides were separated using a 90 min gradient of 3 to 33% acetonitrile in 0.1% formic acid at a flow rate of 200 nL/min (fractionated samples) or a 180 min gradient with otherwise identical parameters (unfractionated sample). Each analysis used a MultiNotch MS3-based TMT method. The scan sequence began with an MS1 spectrum (Orbitrap analysis, resolution 120,000, 400-1400 Thompson, Automatic Gain Control (AGC) target 2×10^5, maximum injection time 50 ms). MS2 analysis consisted of Collision Induced Dissociation (CID) (quadrupole ion trap analysis, AGC 15,000, Normalized Collision Energy (NCE) 35, maximum injection time 120 ms). The top ten precursors were selected for MS3 analysis, in which precursors were fragmented by HCD prior to Orbitrap analysis (NCE 55, max AGC 2×10^5, maximum injection time 150 ms, isolation specificity 0.5 Th, resolution 60,000). Mass spectra were processed using a Sequest-based in-house software pipeline as previously described (56). Data were searched using the human Uniprot database (April 2014) concatenated with common contaminants (56), and filtered to a final protein-level false discovery rate of 1%. Proteins were quantified by summing TMT reporter ion counts across all peptide-spectral matches using an in-house software as previously described (56), excluding peptide-spectral matches with poor quality MS3 spectra (a combined signal:noise ratio of less than 250 across all TMT reporter ions). For protein quantitation, reverse and

contaminant proteins were removed, then each reporter ion channel was summed across all quantified proteins and normalized assuming equal protein loading across all samples. Fold change for each protein was calculated according to (average signal:noise (BSG knockouts) / average signal:noise (JK-1 controls)) or (signal:noise (cRBC sample) / average signal:noise (JK-1 controls)). Protein quantitation values were exported for further analysis in Excel. Gene Ontology Cellular Compartment terms were downloaded from www.uniprot.org and p-values (Significance A) calculated and adjusted with the Benjamini Hochberg method using *Perseus version 1.2.0.16* (95).

Comparison of RBC proteomes

The complete list of 667 proteins identified in the quantitative surface proteomics was compared to published proteomes from the following publications: PMID 16861337 (99), PMID 18346024 (100), PMID 24555563 (101), PMID 22954596 (102), PMID 19778645 (103), PMID 18494517 (104), PMID 18614565 (105), PMID 27006477 (106), PMID 27452463 (57). Datasets were ranked by hierarchical clustering using *Gene Cluster 3.0* (82) with an Euclidian distance similarity metric and visualized using *TreeView v1.1.6r4* (83).

Supplementary Table and Figure Legends

Supplementary Table 1. Table of epigenetic modifiers tested for the ability to induce differentiation of JK-1 cells. This table shows the epigenetic modifiers ranked by cluster analysis. The Cayman Chemicals (https://www.caymanchem.com/Home) catalogue number for each compound is listed. Chemical Abstract Service (CAS) numbers were obtained from Cayman Chemicals or from the *SciFinder* software (https://scifinder.cas.org/). Functional annotation of the targets of each compound was compiled from available literature and the compounds were grouped into the following target categories: histone acetyltransferases, histone deacetylases, histone methyltransferases, histone demethylases, DNA methyltransferases, sirtuins, bromodomains and others.

Supplementary Table 2. Cell surface proteomic analysis of JK-1 WT, Δ*BSG*, *ΔCD44* and cRBC lines. The full list of the 677 proteins identified from the surface proteomics analysis is shown in the 'No_Filter' worksheet. All proteins were identified from the SwissProt database with the exception of PNP, which was identified in the Trembl database. Classification of the identified proteins is given (UniProt ID, Gene Symbol, Description, Gene Ontology Cellular Compartment (GOCC)-term classification: M – membrane, PM – plasma membrane, IPM – integral to plasma membrane, CS – cell surface, XC – extracellular, Nuc – nuclear, ShG – short GO). ''Short GO'' refers to a subset of proteins annotated by GO as "integral component of membrane", but with no subcellular assignment (107). The number of peptides quantified for each protein is shown followed by the fold-change (FC) comparing the average signal:noise (S:N) from the two JK-1 WT samples to either the average S:N from the two *ΔBSG* knockout clones, or to the average S:N from the two *ΔCD44* knockout clones or the S:N from the cRBC sample. The normalized S:N for each protein in JK-1 cells (WT, Δ*BSG*, *ΔCD44*) or cRBCs is finally shown. The 'PM_CS_XC_ShG_2 peptides' worksheet shows all 237 identified plasma membrane proteins, annotated either 'PM', 'CS', 'XC' or 'ShG'. The 'Mapping_Existing_Proteomes' worksheet shows the presence or absence of the 677 proteins identified via surface proteomics with existing published RBC proteomes (indicated via PMID numbers).

Supplementary Figure 1. (**A**) Images of ten different erythroleukemia cell lines during typical in-vitro culture: B4D6 (33); C2F8 (33); Ery-1 (31); HEL92.1.7 (36); K562 (32); LAMA-84 (34); OCIM (37); OCIM-2 (37); TF-1A (35); and JK-1 (22). Scale bars are 20 µm. (**B**) Sorting of cells based on cell size parameter (forward scatter – FSC; side scatter – SSC) leads to the enrichment of differentiated cells in the small cell gate. The relative proportion of the different cell populations is shown in the bar beneath the microscopy image, color coded according to the key in Figure 1A. Scale bars are 10 µm. All cells were stained with May-Grünwald-Giemsa

Supplementary Figure 2. (**A**) GypA levels increase as JK-1 cells differentiate. An undifferentiated population of JK-1 cells was stained with α-GypA-FITC antibody and sorted into GypA-positive and GypA-negative fractions. GypA-negative cells correspond to undifferentiated proerythroblasts while GypA-positive fraction correspond to differentiated polychromatic and orthochromatic cells. Relative proportion of the different cell populations is shown in the bar beneath the microscopy image, color coded according to the key in **Figure 1A**. Scale bar on all images is 10 µm. (**B**) Schematic of the epigenetic library screen. Undifferentiated JK-1 cells were obtained by sorting for α-GypA-negative population at Day 0. Cells were screened for five days (screen 1) or seven and fourteen days (screen 2) and differentiation of JK-1 cells was assessed by measuring the ratio of α-GypA-positive to α-GypA-negative cells. Plots of fold-expansion (**C**) and microscopy images (**D**) for induction with either DMSO control, 2 µM PFI-1, 1 µM (+)-JQ1, or a combination of 2 µM PFI-1 + 1 µM (+)-JQ1. The fold-expansion of the cells is higher in the 2 µM PFI-1 conditions. Addition of (+)-JQ1 alone or in combination with PFI-1 leads to reduced cell expansion

and a more distended cell morphology. Data in (**C**) are average and standard deviation from 2 replicates. Tranylcypromine maintains JK-1 cells in an undifferentiated state. (**E**) Growth curve of JK-1 cells treated with DMSO or with 10 µM tranylcypromine. Data are average and standard deviation of between 3 – 4 biological replicates. (**F**) Treatment of JK-1 cells with 10 µM tranylcypromine maintains the cells in an undifferentiated state (compared to a DMSO-control) as shown by representative flow cytometry plots of cells stained with GypA, CD71 and CD34 over a course of 8 days.

Supplementary Figure 3. Comparison of jkRBC cells to cRBCs and RBCs. (**A**) The longest (D1) and shortest (D2) diameters of day 16 cRBC cells at different stages of erythropoiesis and peripheral RBCs were measured from between 50 – 100 cells using May-Grünwald-Giemsa stained images. The average (indicated value) and standard deviations for each range are shown. (**B**) The relative proportion of erythroid cells from three independent cRBC cultures at 16/17 days post-thaw were measured from between 500 – 800 cells. (**C**) The 677 jkRBC proteins identified by quantitative proteomics were compared to published RBC whole proteome datasets as shown in the heatmap. The presence of a jkRBC protein in a published dataset is indicated by a blue box. The heatmap is split into two, where the right heatmap is a continuation of the bottom of the left heatmap. The following datasets were compared: PMID 16861337 (99), PMID 18346024 (100), PMID 24555563 (101), PMID 22954596 (102), PMID 19778645 (103), PMID 18494517 (104), PMID 18614565 (105), PMID 27006477 (106), PMID 27452463 (57). (**D**) Comparison of fold-change between cRBC and jkRBCs for blood group proteins identified by surface proteomics. The majority of cRBC proteins have relative abundance close to that found in jkRBC with a few exceptions (e.g. BCAM, SLC14A1, CD99). Proteins that are known to be associated with *P. falciparum* invasion are indicated in bold. (**E**) The propensity for multiple invasion events was determined via a selectivity index (SI) (61): higher SI indicates greater number of multiple invasions into a single host cell. The SI of jkRBCs was comparable to cRBCs but higher than RBCs. Average and standard deviation are from four biological replicates.

Supplementary Figure 4. Growth of parasites in jkRBCs is impeded. (**A**) *P. falciparum* strain 3D7 parasites were purified using a Percoll gradient to enrich for late-stage schizonts and parasites were allowed to invade jkRBCs and RBCs for 4 hours at which time heparin was added to block further invasion (76, 108). Parasites were followed over one complete cycle and the proportion of rings, trophozoites and schizonts was evaluated by slide microscopy. Formation of trophozoites and schizonts was observed to be delayed in jkRBCs compared to RBCs. Data represent the average and standard deviation of two biological replicates. (**B**) Representative images of parasites during the experiment with the ring, trophozoite and schizont stage parasites indicated. Scale bar on all images is 10 µm.

Supplementary Figure 5. Genetic manipulation of JK-1 cells.
(**A**) An undifferentiated population of JK-1 cells was transduced with lentivirus targeting either *GYPA* or Luciferase (shLuc) as a control (14, 26). Flow cytometry analysis with α-GypA-FITC staining revealed a ~ 20-fold knockdown (based on comparison of mean fluorescence intensity). (**B**) Generation of CRISPR/Cas9 knockouts and validation of BSG knockout by TIDE (86) analysis. A schematic shows the steps in generating gene knockouts using JK-1 cells. Cells were transduced with a lentivirus containing the LentiCas9-Blast vector and then selected with blasticidin. The single-guide RNA was cloned into LentiGuide-Puro and this vector was transduced into the Cas9-expressing cells and cells were co-selected with blasticidin and puromycin. After two weeks of selection, cells were plated to obtain clones by limiting dilution. Deletions were validated by Sanger sequencing and TIDE analysis. (**C**) The ΔBSG-1 clone has two prominent deletions of -3 bp and -22 bp. (**D**) The ΔBSG-2 clone has two prominent deletions of -2 bp and -8 bp. (**E**) The location of the deletions was mapped based on the Sanger sequencing data and TIDE analysis.

Supplementary Figure 6. Generation of the ΔCD44 knockout line. **(A)** Domain structure of the full-length CD44 protein indicating the N-terminal hyaluronan binding domain in the extracellular region, the single-pass transmembrane helix and the C-terminal cytoplasmic domain. Numbers below the figure represent amino acid positions. **(B)** Exon structure of CD44 and location of the CD44-1 sgRNA binding site. In the ΔCD44-1 and ΔCD44-2 clones we observe single base insertions (indicated in red bold type) that result in a premature stop codon (*) and a truncated protein. Importantly, the truncated protein does not have a transmembrane domain which is located in the C-terminus of the gene. **(C)** Representative microscopy images of wild-type jkRBCs and ΔCD44 knockout cells are shown. Flow cytometry comparison of levels of CD44, BSG, GypA, GypC and CR1 between wild-type and ΔCD44 knockout cells demonstrating specific loss of CD44 signal, while levels of other surface markers remains unaffected. Scale bar on all images is 10 µm. (**D**) Measurement of the relative flow cytometry signals for BSG and GypA in JK-1 WT and ΔCD44-1 knockout line. Average and standard deviation from n = 4 independent experiments.

References

1. WHO (2015) *World Malaria Report 2015* (World Health Organization, Geneva, Switzerland).
2. White NJ*, et al.* (2014) Malaria. *Lancet* 383(9918):723-735.
3. Dvorak JA, Miller LH, Whitehouse WC, & Shiroishi T (1975) Invasion of erythrocytes by malaria merozoites. *Science* 187(4178):748-750.
4. Cowman AF & Crabb BS (2006) Invasion of red blood cells by malaria parasites. *Cell* 124(4):755-766.
5. Weiss GE, Crabb BS, & Gilson PR (2016) Overlaying Molecular and Temporal Aspects of Malaria Parasite Invasion. *Trends in parasitology*.
6. Tham WH, Healer J, & Cowman AF (2012) Erythrocyte and reticulocyte binding-like proteins of Plasmodium falciparum. *Trends in parasitology* 28(1):23-30.
7. Crosnier C*, et al.* (2011) Basigin is a receptor essential for erythrocyte invasion by Plasmodium falciparum. *Nature* 480(7378):534-537.
8. Richards JS & Beeson JG (2009) The future for blood-stage vaccines against malaria. *Immunology and cell biology* 87(5):377-390.
9. Ord RL, Rodriguez M, & Lobo CA (2015) Malaria invasion ligand RH5 and its prime candidacy in blood-stage malaria vaccine design. *Human vaccines & immunotherapeutics* 11(6):1465-1473.
10. Sim BK, Chitnis CE, Wasniowska K, Hadley TJ, & Miller LH (1994) Receptor and ligand domains for invasion of erythrocytes by Plasmodium falciparum. *Science* 264(5167):1941-1944.
11. Crosnier C*, et al.* (2013) A library of functional recombinant cell-surface and secreted P. falciparum merozoite proteins. *Molecular & cellular proteomics : MCP* 12(12):3976-3986.
12. Giarratana MC*, et al.* (2005) Ex vivo generation of fully mature human red blood cells from hematopoietic stem cells. *Nature biotechnology* 23(1):69-74.
13. Giarratana MC*, et al.* (2011) Proof of principle for transfusion of in vitro-generated red blood cells. *Blood* 118(19):5071-5079.
14. Bei AK, Brugnara C, & Duraisingh MT (2010) In vitro genetic analysis of an erythrocyte determinant of malaria infection. *The Journal of infectious diseases* 202(11):1722-1727.
15. Hsu PD, Lander ES, & Zhang F (2014) Development and applications of CRISPR-Cas9 for genome engineering. *Cell* 157(6):1262-1278.
16. Ran FA*, et al.* (2013) Genome engineering using the CRISPR-Cas9 system. *Nature protocols* 8(11):2281-2308.
17. Shalem O*, et al.* (2014) Genome-scale CRISPR-Cas9 knockout screening in human cells. *Science* 343(6166):84-87.
18. Cong L & Zhang F (2015) Genome engineering using CRISPR-Cas9 system. *Methods in molecular biology* 1239:197-217.
19. Sanjana NE, Shalem O, & Zhang F (2014) Improved vectors and genome-wide libraries for CRISPR screening. *Nature methods* 11(8):783-784.
20. Mandal PK*, et al.* (2014) Efficient ablation of genes in human hematopoietic stem and effector cells using CRISPR/Cas9. *Cell stem cell* 15(5):643-652.
21. Hendel A*, et al.* (2015) Chemically modified guide RNAs enhance CRISPR-Cas genome editing in human primary cells. *Nature biotechnology* 33(9):985-989.
22. Okuno Y*, et al.* (1990) Establishment of an erythroid cell line (JK-1) that spontaneously differentiates to red cells. *Cancer* 66(7):1544-1551.
23. Chen L*, et al.* (2014) Crystal structure of PfRh5, an essential P. falciparum ligand for invasion of human erythrocytes. *eLife* 3.
24. Wright KE*, et al.* (2014) Structure of malaria invasion protein RH5 with erythrocyte basigin and blocking antibodies. *Nature* 515(7527):427-430.

25. Douglas AD*, et al.* (2014) Neutralization of Plasmodium falciparum merozoites by antibodies against PfRH5. *Journal of immunology* 192(1):245-258.
26. Egan ES*, et al.* (2015) Malaria. A forward genetic screen identifies erythrocyte CD55 as essential for Plasmodium falciparum invasion. *Science* 348(6235):711-714.
27. Slomiany MG*, et al.* (2009) Hyaluronan, CD44, and emmprin regulate lactate efflux and membrane localization of monocarboxylate transporters in human breast carcinoma cells. *Cancer research* 69(4):1293-1301.
28. Hao J*, et al.* (2010) Co-expression of CD147 (EMMPRIN), CD44v3-10, MDR1 and monocarboxylate transporters is associated with prostate cancer drug resistance and progression. *British journal of cancer* 103(7):1008-1018.
29. Grass GD, Tolliver LB, Bratoeva M, & Toole BP (2013) CD147, CD44, and the epidermal growth factor receptor (EGFR) signaling pathway cooperate to regulate breast epithelial cell invasiveness. *The Journal of biological chemistry* 288(36):26089-26104.
30. Tamez PA, Liu H, Fernandez-Pol S, Haldar K, & Wickrema A (2009) Stage-specific susceptibility of human erythroblasts to Plasmodium falciparum malaria infection. *Blood* 114(17):3652-3655.
31. Ribadeau Dumas A*, et al.* (2004) Establishment and characterization of a new human erythroleukemic cell line, ERY-1. *Leuk Res* 28(12):1329-1339.
32. Lozzio CB & Lozzio BB (1975) Human chronic myelogenous leukemia cell-line with positive Philadelphia chromosome. *Blood* 45(3):321-334.
33. Furukawa T*, et al.* (1994) Establishment of a new cell line with the characteristics of a multipotential progenitor from a patient with chronic myelogenous leukemia in early erythroblastic crisis. *Leukemia* 8(1):171-180.
34. Seigneurin D*, et al.* (1987) Human chronic myeloid leukemic cell line with positive Philadelphia chromosome exhibits megakaryocytic and erythroid characteristics. *Exp Hematol* 15(8):822-832.
35. Hu X*, et al.* (1998) Characterization of a unique factor-independent variant derived from human factor-dependent TF-1 cells: a transformed event. *Leuk Res* 22(9):817-826.
36. Martin P & Papayannopoulou T (1982) HEL cells: a new human erythroleukemia cell line with spontaneous and induced globin expression. *Science* 216(4551):1233-1235.
37. Papayannopoulou T, Nakamoto B, Kurachi S, Tweeddale M, & Messner H (1988) Surface antigenic profile and globin phenotype of two new human erythroleukemia lines: characterization and interpretations. *Blood* 72(3):1029-1038.
38. Kaushansky K*, et al.* (2015) *Williams Hematology, 9th Edition* Ninth edition. Ed p p.
39. Harrison FL, Beswick TM, & Chesterton CJ (1981) Separation of haemopoietic cells for biochemical investigation. Preparation of erythroid and myeloid cells from human and laboratory-animal bone marrow and the separation of erythroblasts according to their state of maturation. *The Biochemical journal* 194(3):789-796.
40. Lotem J & Sachs L (2006) Epigenetics and the plasticity of differentiation in normal and cancer stem cells. *Oncogene* 25(59):7663-7672.
41. Jones PA & Baylin SB (2007) The epigenomics of cancer. *Cell* 128(4):683-692.
42. Lotem J & Sachs L (2002) Epigenetics wins over genetics: induction of differentiation in tumor cells. *Seminars in cancer biology* 12(5):339-346.
43. Hu J*, et al.* (2013) Isolation and functional characterization of human erythroblasts at distinct stages: implications for understanding of normal and disordered erythropoiesis in vivo. *Blood* 121(16):3246-3253.
44. Li J*, et al.* (2014) Isolation and transcriptome analyses of human erythroid progenitors: BFU-E and CFU-E. *Blood* 124(24):3636-3645.
45. Filippakopoulos P*, et al.* (2010) Selective inhibition of BET bromodomains. *Nature* 468(7327):1067-1073.

46. Picaud S*, et al.* (2013) PFI-1, a highly selective protein interaction inhibitor, targeting BET Bromodomains. *Cancer research* 73(11):3336-3346.
47. Gallenkamp D, Gelato KA, Haendler B, & Weinmann H (2014) Bromodomains and their pharmacological inhibitors. *ChemMedChem* 9(3):438-464.
48. Picaud S*, et al.* (2015) Generation of a Selective Small Molecule Inhibitor of the CBP/p300 Bromodomain for Leukemia Therapy. *Cancer research* 75(23):5106-5119.
49. Zucconi BE*, et al.* (2016) Modulation of p300/CBP Acetylation of Nucleosomes by Bromodomain Ligand I-CBP112. *Biochemistry* 55(27):3727-3734.
50. Vangamudi B*, et al.* (2015) The SMARCA2/4 ATPase Domain Surpasses the Bromodomain as a Drug Target in SWI/SNF-Mutant Cancers: Insights from cDNA Rescue and PFI-3 Inhibitor Studies. *Cancer research* 75(18):3865-3878.
51. Verma SK*, et al.* (2012) Identification of Potent, Selective, Cell-Active Inhibitors of the Histone Lysine Methyltransferase EZH2. *ACS medicinal chemistry letters* 3(12):1091-1096.
52. Konze KD*, et al.* (2013) An orally bioavailable chemical probe of the Lysine Methyltransferases EZH2 and EZH1. *ACS chemical biology* 8(6):1324-1334.
53. Kim KH & Roberts CW (2016) Targeting EZH2 in cancer. *Nature medicine* 22(2):128-134.
54. Pan BT & Johnstone RM (1983) Fate of the transferrin receptor during maturation of sheep reticulocytes in vitro: selective externalization of the receptor. *Cell* 33(3):967-978.
55. Liu J, Guo X, Mohandas N, Chasis JA, & An X (2010) Membrane remodeling during reticulocyte maturation. *Blood* 115(10):2021-2027.
56. Weekes MP*, et al.* (2014) Quantitative temporal viromics: an approach to investigate host-pathogen interaction. *Cell* 157(6):1460-1472.
57. Gautier EF*, et al.* (2016) Comprehensive Proteomic Analysis of Human Erythropoiesis. *Cell reports* 16(5):1470-1484.
58. Fernandez-Becerra C*, et al.* (2013) Red blood cells derived from peripheral blood and bone marrow CD34(+) human haematopoietic stem cells are permissive to Plasmodium parasites infection. *Memorias do Instituto Oswaldo Cruz* 108(6):801-803.
59. Walliker D*, et al.* (1987) Genetic analysis of the human malaria parasite Plasmodium falciparum. *Science* 236(4809):1661-1666.
60. Guinet F*, et al.* (1996) A developmental defect in Plasmodium falciparum male gametogenesis. *The Journal of cell biology* 135(1):269-278.
61. Simpson JA, Silamut K, Chotivanich K, Pukrittayakamee S, & White NJ (1999) Red cell selectivity in malaria: a study of multiple-infected erythrocytes. *Transactions of the Royal Society of Tropical Medicine and Hygiene* 93(2):165-168.
62. Spring FA*, et al.* (1997) The Oka blood group antigen is a marker for the M6 leukocyte activation antigen, the human homolog of OX-47 antigen, basigin and neurothelin, an immunoglobulin superfamily molecule that is widely expressed in human cells and tissues. *European journal of immunology* 27(4):891-897.
63. Lamarque M*, et al.* (2011) The RON2-AMA1 interaction is a critical step in moving junction-dependent invasion by apicomplexan parasites. *PLoS pathogens* 7(2):e1001276.
64. Paul AS, Egan ES, & Duraisingh MT (2015) Host-parasite interactions that guide red blood cell invasion by malaria parasites. *Current opinion in hematology* 22(3):220-226.
65. Dhalluin C*, et al.* (1999) Structure and ligand of a histone acetyltransferase bromodomain. *Nature* 399(6735):491-496.
66. Jenuwein T & Allis CD (2001) Translating the histone code. *Science* 293(5532):1074-1080.
67. Florence B & Faller DV (2001) You bet-cha: a novel family of transcriptional regulators. *Frontiers in bioscience : a journal and virtual library* 6:D1008-1018.

68. Filippakopoulos P & Knapp S (2012) The bromodomain interaction module. *FEBS letters* 586(17):2692-2704.
69. Dawson MA*, et al.* (2011) Inhibition of BET recruitment to chromatin as an effective treatment for MLL-fusion leukaemia. *Nature* 478(7370):529-533.
70. Lamonica JM*, et al.* (2011) Bromodomain protein Brd3 associates with acetylated GATA1 to promote its chromatin occupancy at erythroid target genes. *Proceedings of the National Academy of Sciences of the United States of America* 108(22):E159-168.
71. Stonestrom AJ*, et al.* (2015) Functions of BET proteins in erythroid gene expression. *Blood* 125(18):2825-2834.
72. Park A, Won ST, Pentecost M, Bartkowski W, & Lee B (2014) CRISPR/Cas9 allows efficient and complete knock-in of a destabilization domain-tagged essential protein in a human cell line, allowing rapid knockdown of protein function. *PloS one* 9(4):e95101.
73. Salesse S & Verfaillie CM (2002) BCR/ABL: from molecular mechanisms of leukemia induction to treatment of chronic myelogenous leukemia. *Oncogene* 21(56):8547-8559.
74. Lim C*, et al.* (2013) Expansion of host cellular niche can drive adaptation of a zoonotic malaria parasite to humans. *Nature communications* 4:1638.
75. Bustamante LY*, et al.* (2013) A full-length recombinant Plasmodium falciparum PfRH5 protein induces inhibitory antibodies that are effective across common PfRH5 genetic variants. *Vaccine* 31(2):373-379.
76. Weiss GE*, et al.* (2015) Revealing the sequence and resulting cellular morphology of receptor-ligand interactions during Plasmodium falciparum invasion of erythrocytes. *PLoS pathogens* 11(2):e1004670.
77. Paul AS*, et al.* (2015) Parasite Calcineurin Regulates Host Cell Recognition and Attachment by Apicomplexans. *Cell host & microbe* 18(1):49-60.
78. Williams AR*, et al.* (2012) Enhancing blockade of Plasmodium falciparum erythrocyte invasion: assessing combinations of antibodies against PfRH5 and other merozoite antigens. *PLoS pathogens* 8(11):e1002991.
79. Duraisingh MT, Maier AG, Triglia T, & Cowman AF (2003) Erythrocyte-binding antigen 175 mediates invasion in Plasmodium falciparum utilizing sialic acid-dependent and -independent pathways. *Proceedings of the National Academy of Sciences of the United States of America* 100(8):4796-4801.
80. Nunomura W*, et al.* (1997) Regulation of CD44-protein 4.1 interaction by Ca2+ and calmodulin. Implications for modulation of CD44-ankyrin interaction. *The Journal of biological chemistry* 272(48):30322-30328.
81. Aniweh Y*, et al.* (2017) RH5-Basigin interaction induces changes in the cytoskeleton of the host RBC. *Cellular microbiology*.
82. de Hoon MJ, Imoto S, Nolan J, & Miyano S (2004) Open source clustering software. *Bioinformatics* 20(9):1453-1454.
83. Saldanha AJ (2004) Java Treeview--extensible visualization of microarray data. *Bioinformatics* 20(17):3246-3248.
84. Doench JG*, et al.* (2016) Optimized sgRNA design to maximize activity and minimize off-target effects of CRISPR-Cas9. *Nature biotechnology* 34(2):184-191.
85. Moffat J*, et al.* (2006) A lentiviral RNAi library for human and mouse genes applied to an arrayed viral high-content screen. *Cell* 124(6):1283-1298.
86. Brinkman EK, Chen T, Amendola M, & van Steensel B (2014) Easy quantitative assessment of genome editing by sequence trace decomposition. *Nucleic acids research* 42(22):e168.
87. Weekes MP*, et al.* (2013) Latency-associated degradation of the MRP1 drug transporter during latent human cytomegalovirus infection. *Science* 340(6129):199-202.

88. Trager W & Jensen JB (1976) Human malaria parasites in continuous culture. *Science* 193(4254):673-675.
89. Cranmer SL, Magowan C, Liang J, Coppel RL, & Cooke BM (1997) An alternative to serum for cultivation of Plasmodium falciparum in vitro. *Transactions of the Royal Society of Tropical Medicine and Hygiene* 91(3):363-365.
90. Trang DT, Huy NT, Kariu T, Tajima K, & Kamei K (2004) One-step concentration of malarial parasite-infected red blood cells and removal of contaminating white blood cells. *Malaria journal* 3:7.
91. Ribaut C*, et al.* (2008) Concentration and purification by magnetic separation of the erythrocytic stages of all human Plasmodium species. *Malaria journal* 7:45.
92. Lim C*, et al.* (2016) Improved light microscopy counting method for accurately counting Plasmodium parasitemia and reticulocytemia. *American journal of hematology* 91(8):852-855.
93. Brecher G & Schneiderman M (1950) A time-saving device for the counting of reticulocytes. *American journal of clinical pathology* 20(11):1079-1083.
94. Rozenberg G (2011) *Microscopic Haematology : A Practical Guide for the Laboratory (3rd Edition)* (Elsevier Health Sciences Chatswood, NSW, AUS).
95. Cox J & Mann M (2008) MaxQuant enables high peptide identification rates, individualized p.p.b.-range mass accuracies and proteome-wide protein quantification. *Nature biotechnology* 26(12):1367-1372.
96. Aingaran M*, et al.* (2012) Host cell deformability is linked to transmission in the human malaria parasite Plasmodium falciparum. *Cellular microbiology* 14(7):983-993.
97. Coleman BI*, et al.* (2012) Nuclear repositioning precedes promoter accessibility and is linked to the switching frequency of a Plasmodium falciparum invasion gene. *Cell host & microbe* 12(6):739-750.
98. Nkrumah LJ*, et al.* (2006) Efficient site-specific integration in Plasmodium falciparum chromosomes mediated by mycobacteriophage Bxb1 integrase. *Nature methods* 3(8):615-621.
99. Pasini EM*, et al.* (2006) In-depth analysis of the membrane and cytosolic proteome of red blood cells. *Blood* 108(3):791-801.
100. Bosman GJ*, et al.* (2008) The proteome of red cell membranes and vesicles during storage in blood bank conditions. *Transfusion* 48(5):827-835.
101. Lange PF, Huesgen PF, Nguyen K, & Overall CM (2014) Annotating N termini for the human proteome project: N termini and Nalpha-acetylation status differentiate stable cleaved protein species from degradation remnants in the human erythrocyte proteome. *Journal of proteome research* 13(4):2028-2044.
102. Pesciotta EN*, et al.* (2012) A label-free proteome analysis strategy for identifying quantitative changes in erythrocyte membranes induced by red cell disorders. *Journal of proteomics* 76 Spec No.:194-202.
103. van Gestel RA*, et al.* (2010) Quantitative erythrocyte membrane proteome analysis with Blue-native/SDS PAGE. *Journal of proteomics* 73(3):456-465.
104. Ringrose JH*, et al.* (2008) Highly efficient depletion strategy for the two most abundant erythrocyte soluble proteins improves proteome coverage dramatically. *Journal of proteome research* 7(7):3060-3063.
105. Roux-Dalvai F*, et al.* (2008) Extensive analysis of the cytoplasmic proteome of human erythrocytes using the peptide ligand library technology and advanced mass spectrometry. *Molecular & cellular proteomics : MCP* 7(11):2254-2269.
106. Wilson MC*, et al.* (2016) Comparison of the Proteome of Adult and Cord Erythroid Cells, and Changes in the Proteome Following Reticulocyte Maturation. *Molecular & cellular proteomics : MCP* 15(6):1938-1946.

1079 107. Weekes MP*, et al.* (2012) Proteomic plasma membrane profiling reveals an essential role for gp96
1080 in the cell surface expression of LDLR family members, including the LDL receptor and LRP6.
1081 *Journal of proteome research* 11(3):1475-1484.
1082 108. Boyle MJ, Richards JS, Gilson PR, Chai W, & Beeson JG (2010) Interactions with heparin-like
1083 molecules during erythrocyte invasion by Plasmodium falciparum merozoites. *Blood*
1084 115(22):4559-4568.

Figure 1

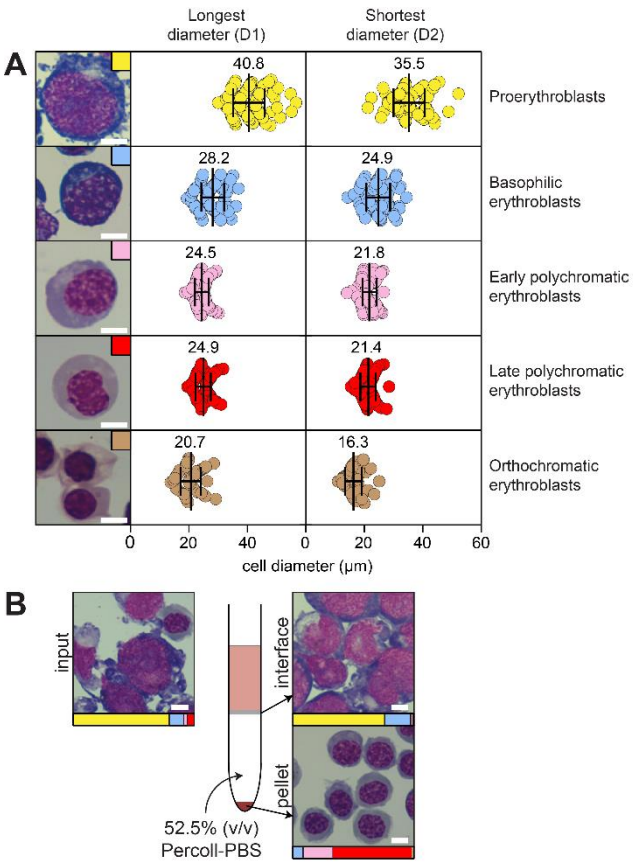

Figure 2

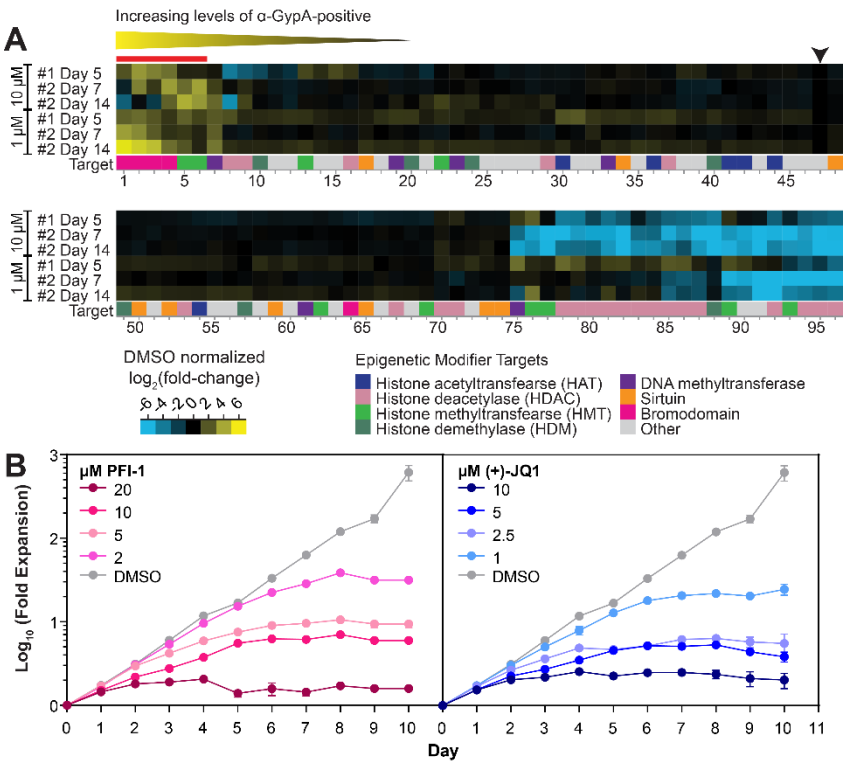

Figure 3

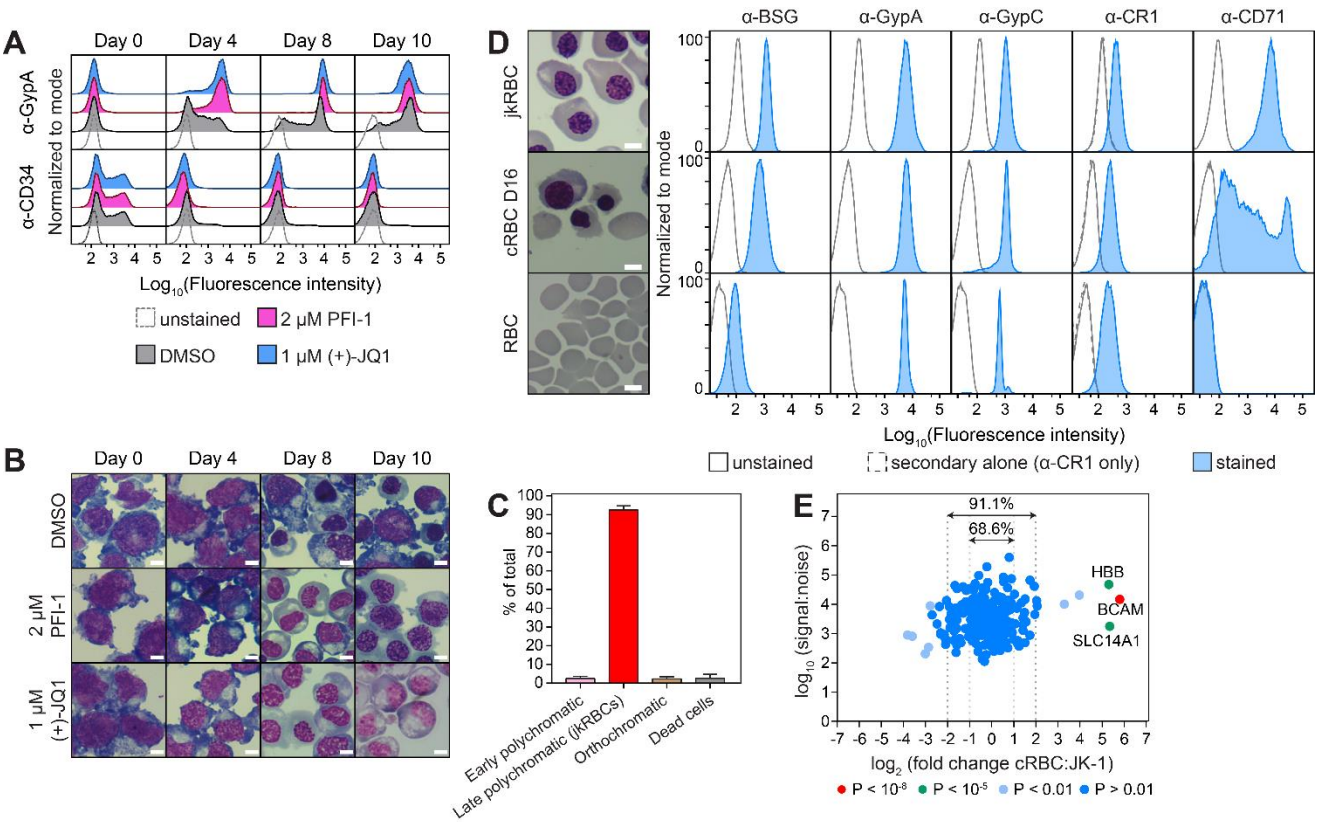

Figure 4

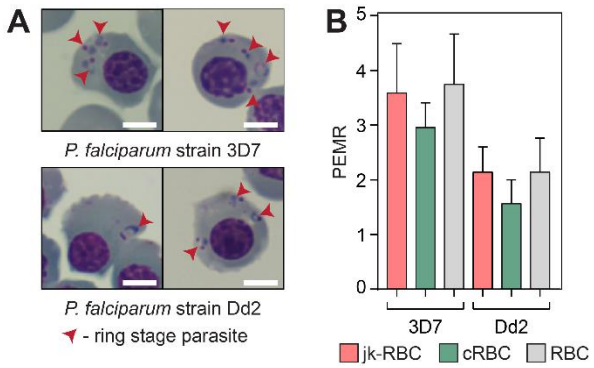

Figure 5

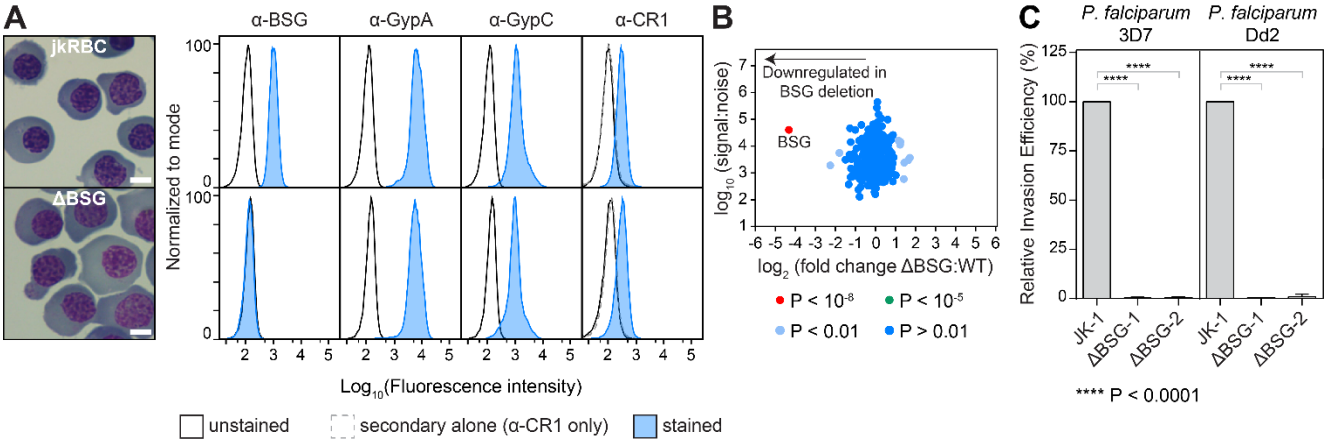

Figure 6

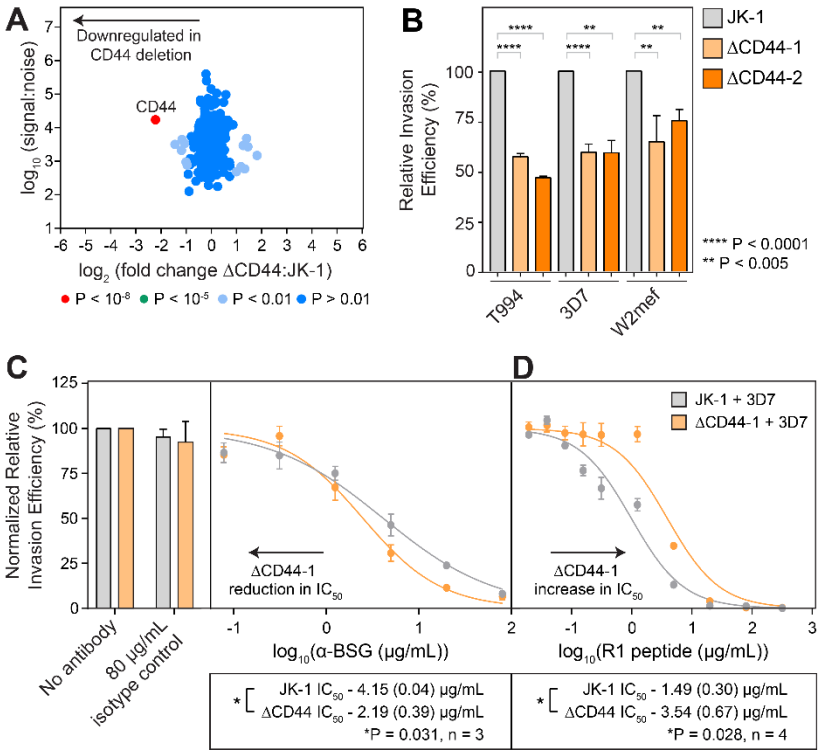
A
Downregulated in CD44 deletion
CD44
log10 (signal:noise)
log2 (fold change ΔCD44:JK-1)
P < 10-8
P < 10-5
P < 0.01
P > 0.01
B
Relative Invasion Efficiency (%)
JK-1
ΔCD44-1
ΔCD44-2
**** P < 0.0001
** P < 0.005
T994
3D7
W2mef
C
Normalized Relative Invasion Efficiency (%)
No antibody
80 μg/mL isotype control
ΔCD44-1 reduction in IC50
log10(α-BSG (μg/mL))
JK-1 IC50 - 4.15 (0.04) μg/mL
ΔCD44 IC50 - 2.19 (0.39) μg/mL
*P = 0.031, n = 3
D
JK-1 + 3D7
ΔCD44-1 + 3D7
ΔCD44-1 increase in IC50
log10(R1 peptide (μg/mL))
JK-1 IC50 - 1.49 (0.30) μg/mL
ΔCD44 IC50 - 3.54 (0.67) μg/mL
*P = 0.028, n = 4

Figure S1

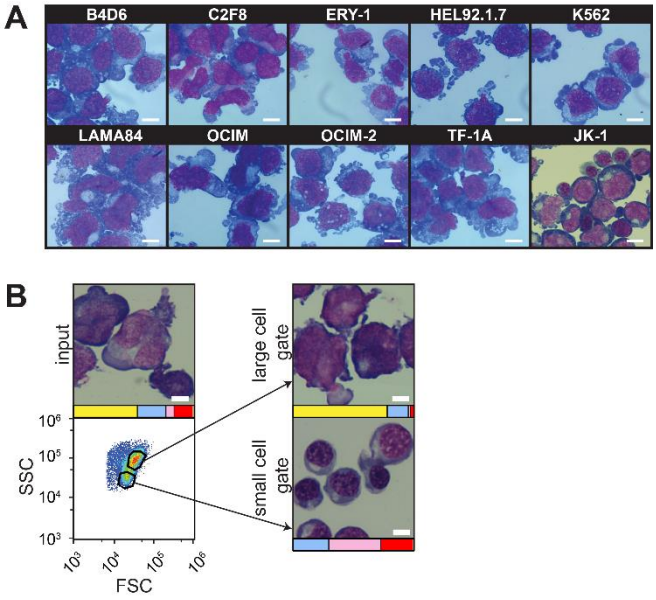
A
B4D6
C2F8
ERY-1
HEL92.1.7
K562
LAMA84
OCIM
OCIM-2
TF-1A
JK-1
B
input
large cell gate
small cell gate
SSC
FSC
10^3
10^4
10^5
10^6

Figure S2

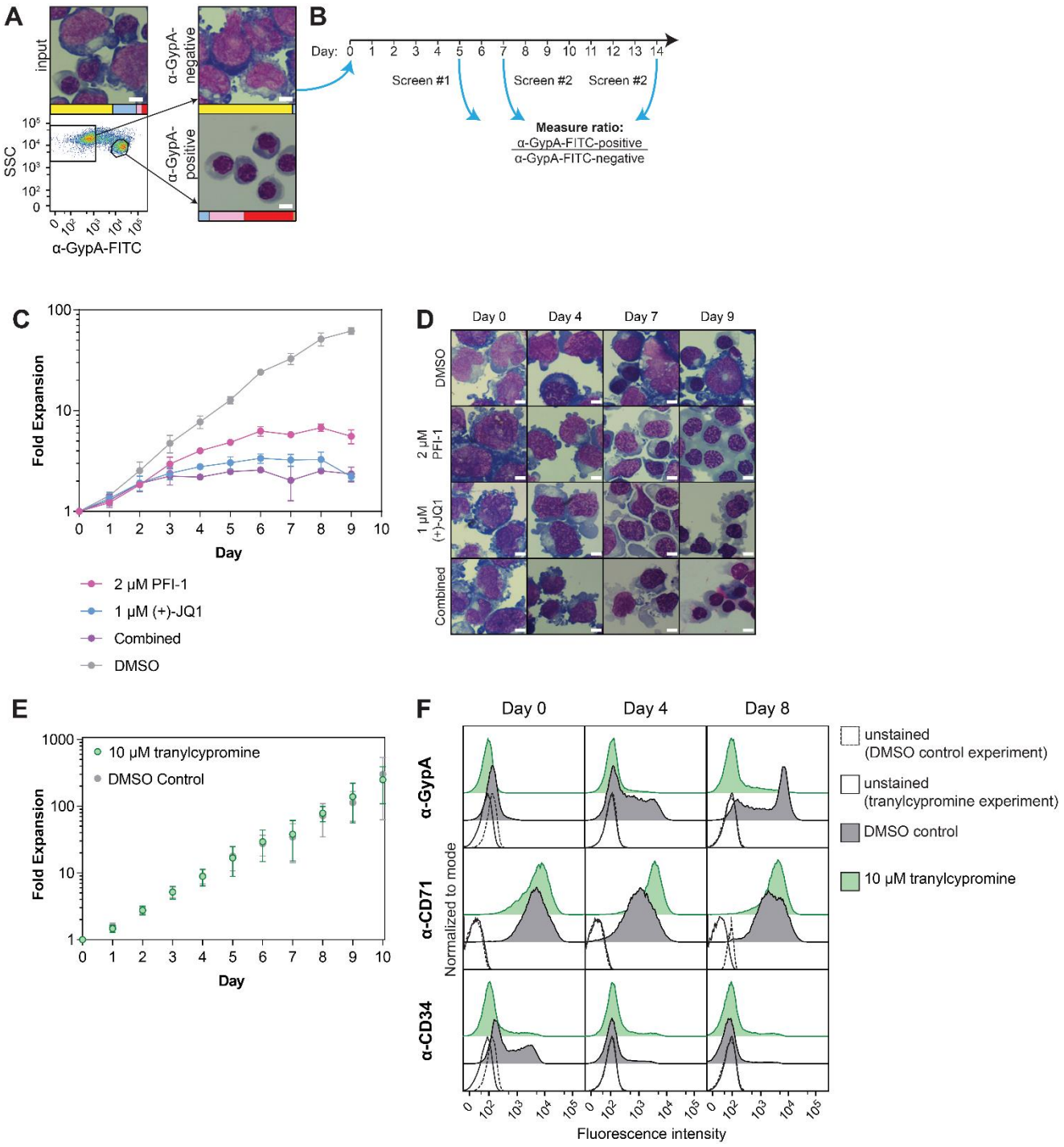
A
input
α-GypA-negative
α-GypA-positive
SSC
α-GypA-FITC
B
Day: 0 1 2 3 4 5 6 7 8 9 10 11 12 13 14
Screen #1
Screen #2
Screen #2
Measure ratio:
α-GypA-FITC-positive
α-GypA-FITC-negative
C
Fold Expansion
Day
2 μM PFI-1
1 μM (+)-JQ1
Combined
DMSO
D
Day 0
Day 4
Day 7
Day 9
DMSO
2 μM PFI-1
1 μM (+)-JQ1
Combined
E
10 μM tranylcypromine
DMSO Control
Fold Expansion
Day
F
Day 0
Day 4
Day 8
α-GypA
α-CD71
α-CD34
Normalized to mode
Fluorescence intensity
unstained (DMSO control experiment)
unstained (tranylcypromine experiment)
DMSO control
10 μM tranylcypromine

Figure S3

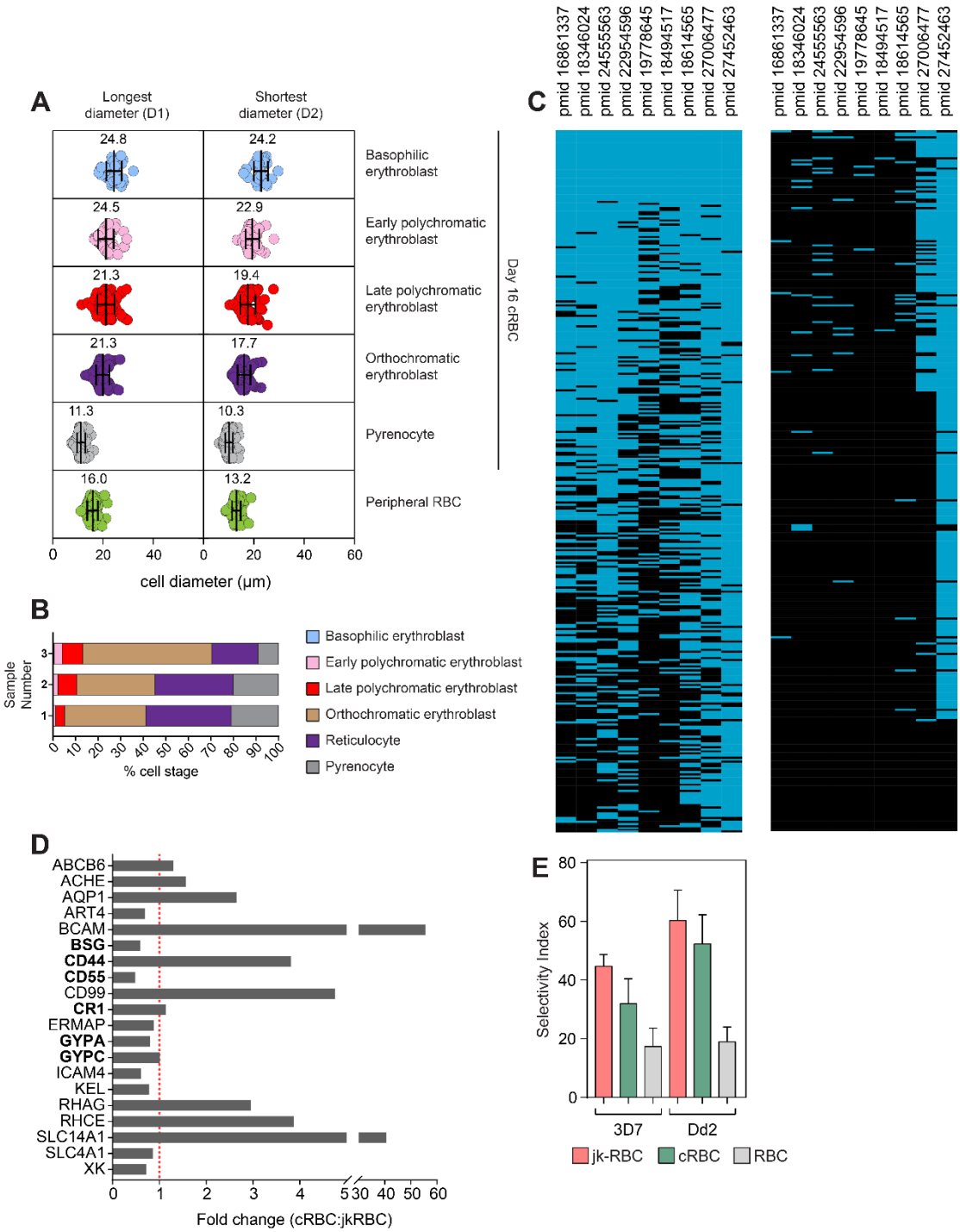
A
Longest diameter (D1)
Shortest diameter (D2)
24.8
24.2
Basophilic erythroblast
24.5
22.9
Early polychromatic erythroblast
21.3
19.4
Late polychromatic erythroblast
21.3
17.7
Orthochromatic erythroblast
11.3
10.3
Pyrenocyte
16.0
13.2
Peripheral RBC
Day 16 cRBC
0 20 40 0 20 40 60
cell diameter (µm)
B
Sample Number
3
2
1
0 10 20 30 40 50 60 70 80 90 100
% cell stage
Basophilic erythroblast
Early polychromatic erythroblast
Late polychromatic erythroblast
Orthochromatic erythroblast
Reticulocyte
Pyrenocyte
C
pmid 16861337
pmid 18346024
pmid 24555563
pmid 22954596
pmid 19778645
pmid 18494517
pmid 18614565
pmid 27006477
pmid 27452463
D
ABCB6
ACHE
AQP1
ART4
BCAM
BSG
CD44
CD55
CD99
CR1
ERMAP
GYPA
GYPC
ICAM4
KEL
RHAG
RHCE
SLC14A1
SLC4A1
XK
0 1 2 3 4 5 30 40 50 60
Fold change (cRBC:jkRBC)
E
Selectivity Index
0 20 40 60 80
3D7
Dd2
jk-RBC
cRBC
RBC

Figure S4

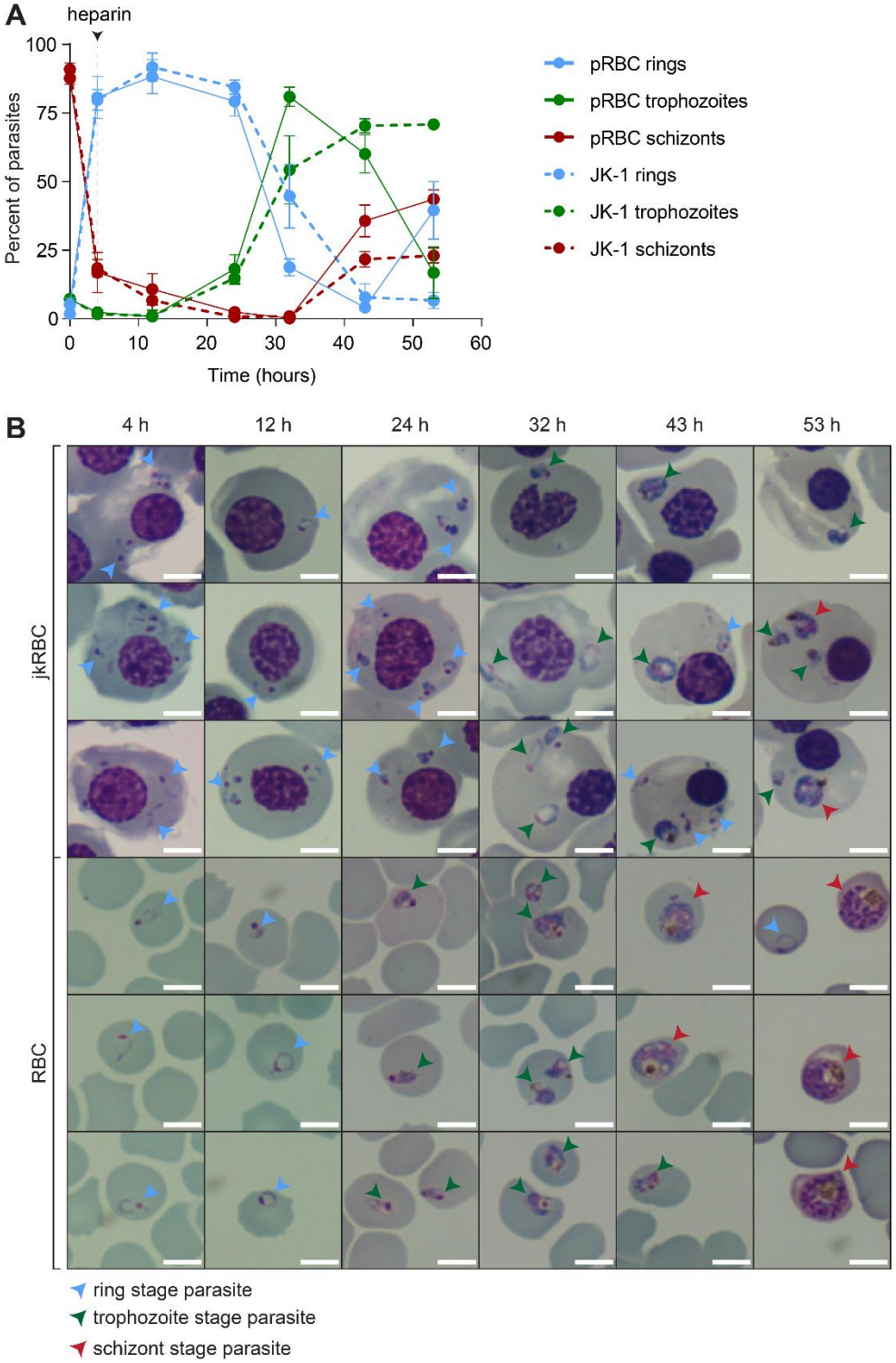
A
heparin
100
75
50
25
0
Percent of parasites
0
10
20
30
40
50
60
Time (hours)
pRBC rings
pRBC trophozoites
pRBC schizonts
JK-1 rings
JK-1 trophozoites
JK-1 schizonts
B
4 h
12 h
24 h
32 h
43 h
53 h
jkRBC
RBC
ring stage parasite
trophozoite stage parasite
schizont stage parasite

Figure S5

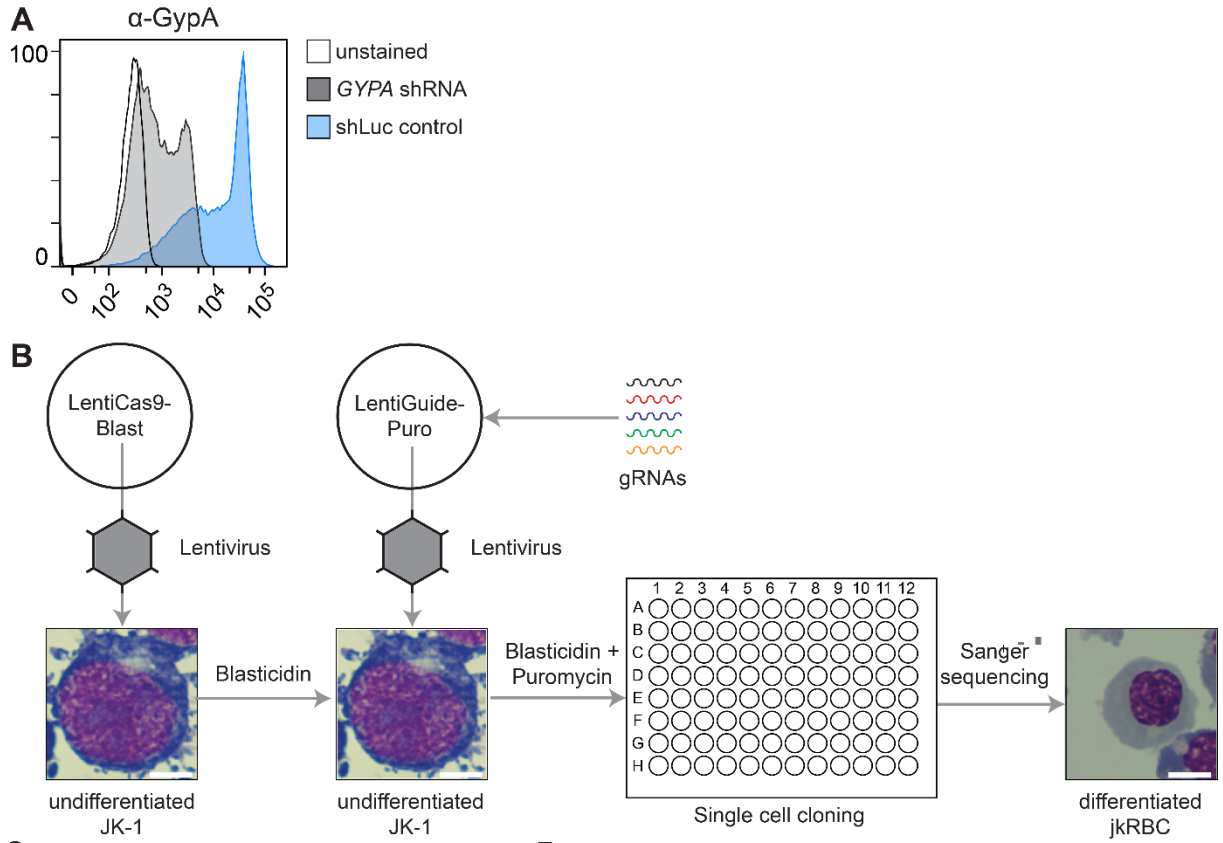
A
α-GypA
100
0
0
10^2
10^3
10^4
10^5
unstained
GYPA shRNA
shLuc control
B
LentiCas9-Blast
LentiGuide-Puro
gRNAs
Lentivirus
Lentivirus
Blasticidin
Blasticidin + Puromycin
Sanger sequencing
1 2 3 4 5 6 7 8 9 10 11 12
A
B
C
D
E
F
G
H
undifferentiated JK-1
undifferentiated JK-1
Single cell cloning
differentiated jkRBC

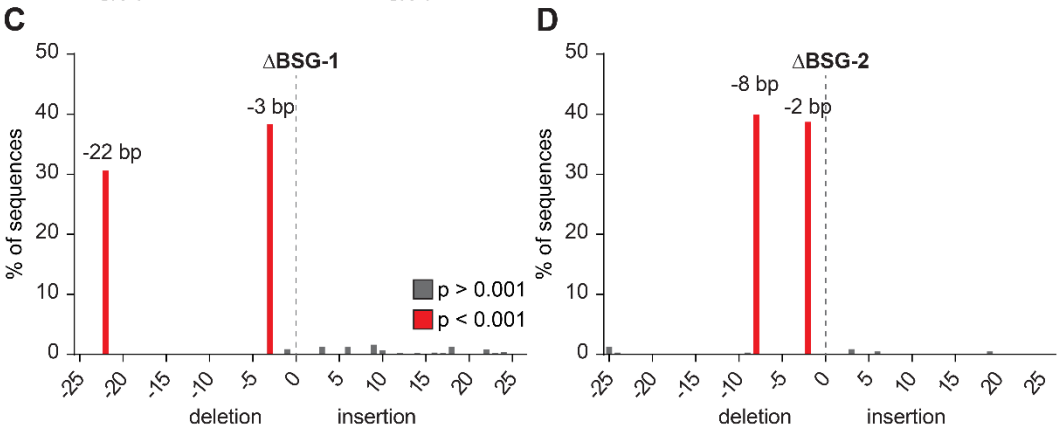
C
ΔBSG-1
-3 bp
-22 bp
% of sequences
p > 0.001
p < 0.001
deletion
insertion
D
ΔBSG-2
-8 bp
-2 bp
% of sequences
deletion
insertion

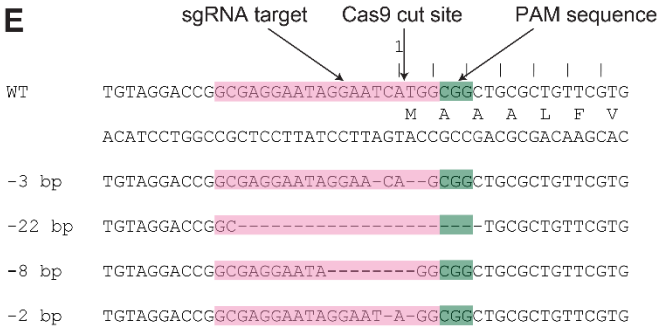
E
sgRNA target
Cas9 cut site
PAM sequence
WT TGTAGGACCGGCGAGGAATAGGAATCATGGCGGCTGCGCTGTTCGTG
M A A A L F V
ACATCCTGGCCGCTCCTTATCCTTAGTACCGCCGACGCGACAAGCAC
-3 bp TGTAGGACCGGCGAGGAATAGGAA-CA--GCGGCTGCGCTGTTCGTG
-22 bp TGTAGGACCGGC----------GCGGCTGCGCTGTTCGTG
-8 bp TGTAGGACCGGCGAGGAATA--------GGCGGCTGCGCTGTTCGTG
-2 bp TGTAGGACCGGCGAGGAATAGGAAT-A-GGCGGCTGCGCTGTTCGTG

Figure S6

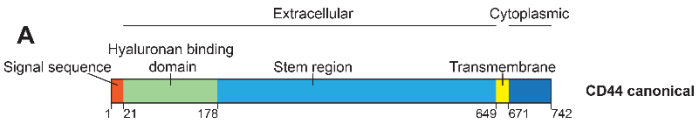
A
Extracellular
Cytoplasmic
Hyaluronan binding domain
Signal sequence
Stem region
Transmembrane
CD44 canonical
1
21
178
649
671
742

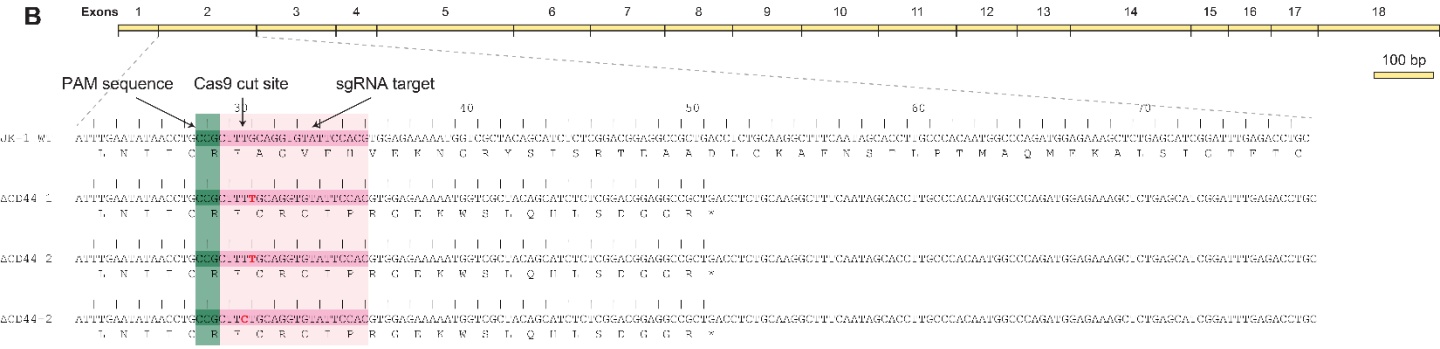
B
Exons 1 2 3 4 5 6 7 8 9 10 11 12 13 14 15 16 17 18
100 bp
PAM sequence
Cas9 cut site
sgRNA target
JK-1 WT
ΔCD44-1
ΔCD44-2
ΔCD44-2

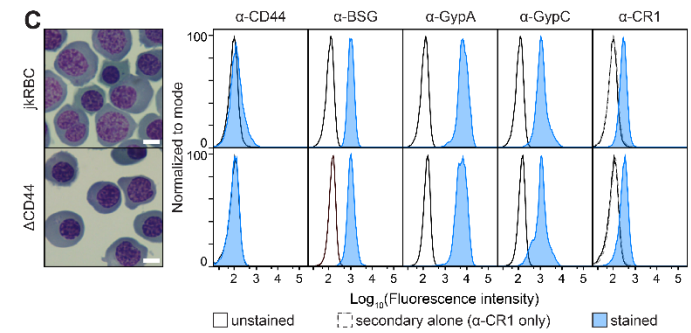
C
jkRBC
ΔCD44
α-CD44
α-BSG
α-GypA
α-GypC
α-CR1
Normalized to mode
100
0
Log10(Fluorescence intensity)
unstained
secondary alone (α-CR1 only)
stained

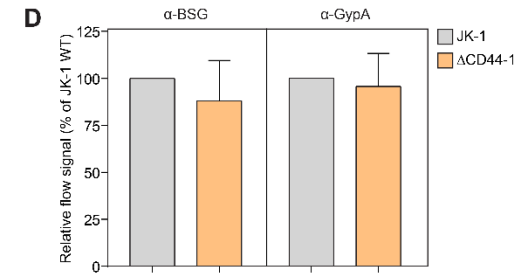
D
α-BSG
α-GypA
JK-1
ΔCD44-1
Relative flow signal (% of JK-1 WT)
125
100
75
50
25
0